Free Radical Biology and Medicine 165 (2021) 368–384

Contents lists available at ScienceDirect

Free Radical Biology and Medicine

journal homepage: www.elsevier.com/locate/freeradbiomed

Original article

Redox sensor NPGPx restrains ZAP70 activity and modulates T cell homeostasis

Fang-Yi Su [a,b], Shih-Chia Huang [a], Pei-Chi Wei [a], Pang-Hung Hsu [b,c], Ju-Pi Li [d,e], Li-Wen Su [a], Yung-Lin Hsieh [a], Chun-Mei Hu [a], Jye-Lin Hsu [f,g], Cheng-Yuan Yang [a], Chen-Yen Chung [h], Jin-Yuh Shew [a], Joung-Liang Lan [d], Huey-Kang Sytwu [i,j], Eva Y-HP Lee [k], Wen-Hwa Lee [a,g,k,*]

[a] Genomics Research Center, Academia Sinica, Taipei, Taiwan
[b] Institute of Biochemistry and Molecular Biology, National Yang-Ming University, Taipei, Taiwan
[c] Department of Bioscience and Biotechnology, National Taiwan Ocean University, Keelung, Taiwan
[d] Division of Rheumatology and Immunology and Department of Internal Medicine, China Medical University Hospital, Taichung, Taiwan
[e] School of Chinese Medicine, China Medical University, Taichung, Taiwan
[f] Graduate Institute of Biomedical Sciences, China Medical University, Taichung, Taiwan
[g] Drug Development Research Center, China Medical University, Taichung, Taiwan
[h] Institute of Biomedical Sciences, Academia Sinica, Taipei, Taiwan
[i] Department and Graduate Institute of Microbiology and Immunology, National Defense Medical Center, Taipei, Taiwan
[j] National Institute of Infectious Diseases and Vaccinology, National Health Research Institutes, Zhunan, Taiwan
[k] Department of Biological Chemistry, University of California, Irvine, Irvine, CA, USA

ARTICLE INFO

Keywords:
T cell
Redox regulation
Autoimmunity
TCR signaling
ZAP70
Glutathione peroxidase

ABSTRACT

Emerging evidences implicate the contribution of ROS to T cell activation and signaling. The tyrosine kinase, ζ-chain-associated protein of 70 kDa (ZAP70), is essential for T cell development and activation. However, it remains elusive whether a direct redox regulation affects ZAP70 activity upon TCR stimulation. Here, we show that deficiency of non-selenocysteine containing phospholipid hydroperoxide glutathione peroxidase (NPGPx), a redox sensor, results in T cell hyperproliferation and elevated cytokine productions. T cell-specific NPGPx-knockout mice reveal enhanced T-dependent humoral responses and are susceptible to experimental autoimmune encephalomyelitis (EAE). Through proteomic approaches, ZAP70 is identified as the key interacting protein of NPGPx through disulfide bonding. NPGPx is activated by ROS generated from TCR stimulation, and modulates ZAP70 activity through redox switching to reduce ZAP70 recruitment to TCR/CD3 complex in membrane lipid raft, therefore subduing TCR responses. These results reveal a delicate redox mechanism that NPGPx serves as a modulator to curb ZAP70 functions in maintaining T cell homeostasis.

1. Introduction

Reactive oxygen species (ROS) are highly unstable by-products generated from oxidative respiration and can damage cellular components [1]. Rather than the detrimental effects, moderate amounts of ROS can modify signal transduction and metabolism through reversible thiol-oxidation of cysteine residues in target proteins to enable biological switching of protein structure and reactivity [2,3]. These post-translational oxidative modifications of cysteine proteome and antioxidant systems build up a delicate redox regulatory mechanism to maintain cellular homeostasis [4]. Several studies have demonstrated that redox imbalance correlates with inflammatory diseases and autoimmune development [5–7], indicating the importance of redox regulation in immune homeostasis.

In T cells, T cell receptor (TCR) stimulation immediately promotes a large amount of ROS production from NADPH oxidases or oxidative respiration chain in mitochondria [8–10]. These ROS function as the positive feedback loops to enhance and sustain TCR signaling through boosting lipid raft formation, inactivating non-receptor tyrosine phosphatases, and cooperating with calcium transients [11–13]. Moreover, despite having positive effects in TCR signaling, recent studies demonstrated that prolonged ROS signaling could lead to T cell hyporeponsiveness and impaired inflammatory responses [14–16]. These observations suggest that a delicate redox regulatory mechanism is crucial for preserving the integrity of T cell-mediated immunity.

* Corresponding author. Genomics Research Center, Academia Sinica, Taipei, Taiwan.
E-mail address: whlee@uci.edu (W.-H. Lee).

https://doi.org/10.1016/j.freeradbiomed.2021.01.013
Received 29 November 2020; Received in revised form 2 January 2021; Accepted 7 January 2021
Available online 16 January 2021

Abbreviations

ANA	Anti-nuclear antibody
$B^{\Delta NPGPx/\Delta NPGPx}$	B-specific NPGPx knockout (*CD19-Cre; NPGPx*$^{fx/fx}$)
DCFDA	oxidation-sensitive dye dichlorodihydro-fluorescein diacetate
EAE	experimental autoimmune encephalomyelitis
GPx	glutathione peroxidase
I-A	interdomain A
I–B	interdomain B
IFN-γ	interferon-γ
IgG	immunoglobulin G
IL-17A	interleukin-17A
IL-2	interleukin-2
IL-4	interleukin-4
IP–MS	immunoprecipitation coupled with mass spectrometry
ITAMs	immunoreceptor tyrosine-based activation motifs
KEGG	Kyoto Encyclopedia of Genes and Genomes
KinD	kinase catalytic domain
NP-KLH	nitrophenol-coupled keyhole limpet hemocyanin
LAT	linker for activation of T cells
NP-LPS	nitrophenol-coupled lipopolysaccharides
MOG	myelin oligodendrocyte protein
NP	4-hydroxy-3-nitrophenylacetyl
NPGPx	non-selenocysteine containing phospholipid hydroperoxide glutathione peroxidase
NPGPx C2S2	Cys-to-Ser double mutant in Cys57 and Cys86 of NPGPx
NPGPx WT	wild-type NPGPx
NPGPx$^{-/-}$	whole-body NPGPx knockout
oxNPGPx	oxidized NPGPx
PBMC	peripheral blood mononuclear cell
PLA	proximity ligation assay
PMA	phorbol myristate acetate
PTK	protein tyrosine kinase
PTP	phosphatase
ROS	reactive oxygen species
SCID	severe combined immunodeficiency
SLE	systemic lupus erythematosus
Syk	spleen tyrosine kinase
TCR	T cell receptor
Treg	regulatory T cell
tSH2	tandem SH2 domains
$T^{\Delta NPGPx/\Delta NPGPx}$	T-specific NPGPx knockout (*CD4-Cre; NPGPx*$^{fx/fx}$)
ZAP70	ζ-chain-associated protein of 70 kDa

Although emerging evidence implicates the contribution of ROS to T cell immune metabolism and signaling [15,17–19], how these ROS are transmitted precisely and whether that in turn affects the essential signaling molecules through oxidative thiol modification to fine-tune TCR responses remain elusive.

It is noted that ZAP70, a TCR-ζ-chain-associated 70 kDa tyrosine kinase, is essential for T cell development and activation [20,21]. Accordingly, ZAP70 deficiency leads to severe combined immunodeficiency (SCID) in both human and mice [22–26]. ZAP70 contains two tandem SH2 domains (tSH2) for phosphopeptide recognition, a kinase catalytic domain (KinD) for phosphotransferation to downstream substrates, and two linker regions, defined as interdomain A (I-A) and interdomain B (I–B) [27]. After peptide-MHC (pMHC) and TCR engagement, the tSH2 of cytosolic ZAP70 is recruited to the plasma membrane by phosphorylated immunoreceptor tyrosine-based activation motifs (ITAMs) present in the TCR-associated CD3 complex, which leading to the release of ZAP70 from its autoinhibited conformation and in turn enable LCK-mediated phosphorylation for stabilizing of active enzyme in an opening form [20,21]. The membrane-located ZAP70 further activates the adaptor protein linker for activation of T cells (LAT) in lipid raft, subsequently promoting F-actin-dependent TCR cluster formation, and results in a signaling microcluster formation for extending T cell activation [28,29]. These studies have elaborated the autoinhibition and activation mechanism of ZAP70. Despite human ZAP70 contains seventeen cysteine residues and two of them are highly conserved throughout the protein tyrosine kinase (PTK) family [30], whether ZAP70 could be directly regulated by oxidative thiol modification during TCR stimulation remains to be elucidated.

Non-selenocysteine containing phospholipid hydroperoxide glutathione peroxidase (NPGPx), also known as GPx7, is one of the eight glutathione peroxidase (GPx) family members and functions as an oxidative stress sensor/transducer [31,32] involving in cellular redox regulation. Unlike other GPx homologs using GSH as cofactor to detoxify cellular oxidative stress, NPGPx senses and transmits oxidative signals by transferring the disulfide bonding between its Cys57 and Cys84 residues to downstream effectors, such as GRP78, PDI, and CPEB2 [31,33,34]. Interestingly, NPGPx-deficient mice revealed accumulated oxidative stress and developed glomerulonephritis with antibody deposition in kidney [31], implicating a possible role of NPGPx in immune homeostasis.

In this communication, we reported that NPGPx deficiency of T cell resulted in hyperactivation, enhanced T-dependent humoral immunity, and was susceptible to experimental autoimmune encephalomyelitis (EAE) induction in mice. Using proteomic approaches, ZAP70 was identified as the key interacting protein with NPGPx through disulfide bonding upon TCR stimulation. NPGPx-mediated redox switching of ZAP70 restrained its TCR/CD3 binding ability, thus preventing its enzymatic activation and subduing TCR response. These results strongly suggested the link between redox machinery and proximal TCR signaling for modulating T cell homeostasis.

2. Materials and methods

2.1. Mice

Mice were maintained in a SPF (specific pathogen-free) animal facility at 20 ± 2 °C with a 12/12 h light/dark cycle and had free access to water and standard laboratory chow diet (LabDiet 5053). The genotype of the off spring was determined by PCR analysis. Female mice with 8-12 weeks in age were used and randomly assigned to all animal experiments. *NPGPx*$^{-/-}$ mice were generated using gene targeting strategy as previous described [31]. For generating C57BL/6J congenic mice, *NPGPx*$^{+/-}$ mice in C57BL/6J x 129/Ola mixed background were backcrossed to C57BL/6J background for twelve generations. C57BL/6J congenic homozygous *NPGPx* knockout (*NPGPx*$^{-/-}$) mice and wild-type littermates (*NPGPx*$^{+/+}$) were obtained by intercross of F12 heterozygotes. The *NPGPx*$^{fx/fx}$ mice were generated as described in Supplementary Materials. *CD4-Cre; NPGPx*$^{fx/fx}$ mice and *CD19-Cre; NPGPx*$^{fx/fx}$ mice were generated by crossing *NPGPx*$^{fx/fx}$ mice to *CD4-Cre* transgenic mice [35] and *CD19-Cre* transgenic mice [36] respectively. *CD4-Cre* mice were obtained from Dr. Ming-Zong Lai (Academia Sinica, Taiwan) purchased from Taconic Farms (Hudson, NY). *CD19-Cre* mice were obtained from Dr. Kuo-I Lin (Academia Sinica, Taiwan).

2.2. Animal immunization

To examine the T-dependent or T-independent humoral responses, mice were intraperitoneal injected with 100 μg nitrophenol-coupled

keyhole limpet hemocyanin (NP-KLH, Biosearch Technologies Inc.) emulsified in Alum adjuvant (Thermo Scientific) or 50 μg nitrophenol-coupled lipopolysaccharide (NP-LPS, Biosearch Technologies Inc.) in PBS, respectively. The production of NP-specific antibodies in sera from immunized mice was assessed by ELISA. EAE was induced by subcutaneous injection at the hind limbs of 8- to 12-week-old female mice with 50 μg myelin oligodendrocyte protein (MOG_{35-55}) peptides emulsified in 200 μg complete Freund's adjuvant (Sigma). Mice were also injected i.p. with 200 ng pertussis toxin (Sigma) on days 0 and 2. All mice were monitored daily for EAE symptoms and were assigned scores on a scale of 0–5 as follows: 0, no overt signs of disease; 1, flaccid tail; 2, flaccid tail and partial hindlimb paralysis; 3, complete hindlimb paralysis; 4, complete hindlimb and partial forelimb paralysis; and 5, moribund state or death. To examine the infiltrating Th cells in spinal cord and the cytokine productions in serum, mice were sacrificed at day 12 or 14 after immunization. The isolation of infiltrating cells in the spinal cord was followed as previous described [37]. To determine the activation of MOG-specific T cells, mice were immunized subcutaneously at the hind limbs with 50 μg myelin oligodendrocyte protein (MOG_{35-55}) peptides emulsified in 200 μg complete Freund's adjuvant (Sigma). Ten days after immunization, mice were sacrificed and splenocytes were harvested and subjected to MOG-antigen restimulation. Cohoused littermate mice were used in these animal studies.

2.3. Isolation of primary cells, ex vivo cell stimulation and activation

Primary $CD4^+$ T, $CD8^+$ T, and B cells were isolated from the lymph nodes and spleens of indicated mice using EasyStep™ mouse $CD4^+$ T, $CD8^+$ T, and B cell isolation kit (STEMCELL Technologies Inc.). Bone marrow-derived macrophages and dendritic cells were harvested as previously described [38,39]. Purified mouse $CD4^+$ T and $CD8^+$ T cells were untreated or stimulated with indicated concentration of plate-bound anti-mouse CD3 (145-2C11; BD Pharmingen) plus 1 μg/ml soluble anti-mouse CD28 (37.51; BD Pharmingen) or phorbol myristate acetate (PMA, 50 ng/ml; Sigma) plus ionomycin (1 μM; Sigma). The culture supernatants were harvested after 24 or 72 h of stimulation and subjected to ELISA analysis to detect cytokine productions. For T cell proliferation assays, isolated $CD4^+$ T and $CD8^+$ T were stained with 5 μM carboxyfluorescein diacetate succinimidyl diester (CFSE; Thermo) and stimulated with indicated treatments for 48 or 72 h followed by flow cytometry analysis. For IL-2 production assay, Jurkat T cells (clone E6-1, TIB-152™; ATCC) and P116 cells (CRL-2676™; ATCC) were stimulated with indicated concentration of plate-bound anti-human CD3 (OKT3; BioXCell) and 1 μg/ml soluble anti-human CD28 (CD28.2; BD Pharmingen) plus PMA (250 ng/ml). The culture supernatants were harvested after 24 h of stimulation to detect the IL-2 production. For the induction of T cell activation, P116 cells were stained with soluble anti-human CD3 (OKT3; 1 μg/ml) for 10 min on ice, following washed and stimulated by $F(ab')_2$ fragment donkey anti-mouse IgG (5 μg/ml; Jackson ImmunoResearch) crosslinking for indicated time points at 37 °C. For TCR signaling analysis, primary isolated $CD4^+$ T cells were stimulated with anti-mouse CD3 (20 μg/ml), anti-mouse CD28 (4 μg/ml), and protein G' (20 μg/ml) for indicated time points at 37 °C.

2.4. Cell lines, transfection and lentiviral transfection

Human Jurkat T leukemia cells (clone E6-1; American Type Cell Culture(ATCC): TIB-152) and their variant, P116 cells (ATCC: CRL-2676), were cultured in RPMI-1640 medium (Thermo) containing 10% Hyclone® fetal bovine serum (FBS; Thermo) plus 1X Gibco™ Non-Essential Amino Acids Solution (Thermo), 1 mM Gibco™ Sodium Pyruvate (Thermo), and 1X Gibco™ Antibiotic-Antimycotic (Thermo). HEK293T cells (ATCC: CRL-11268) were cultured in DMEM medium (Invitrogen) containing 10% FBS plus 1X Antibiotic-Antimycotic. All the cells were free of mycoplasma contamination. Plasmids were transfected into HEK293T cells using TransIT®-LT1 Transfection Reagent (Mirus Bio). The lentiviral particles were produced according to the manufacturer's instructions (National RNAi Core Facility, Taiwan). For reconstituted expression of NPGPx and ZAP70, P116 cells were infected twice with lentiviral particles carrying wild-type or Cys-to-Ser mutant *NPGPx* and *ZAP70* genes in the presence of 10 μg/ml polybrene. The RFP and GFP double-positive cells indicating the successful *NPGPx* and *ZAP70* gene insertion were sorted by FACSAria II Cell Sorter (BD Biosciences). The sorted cells were cultured for additional three passages before formal experiments.

2.5. Cell proliferation analysis

For analysis of cell proliferation, primary isolated $CD4^+$ T or $CD8^+$ T were labeled with 5 mM CFSE (carboxyfluorescein diacetate succinimidyl ester; Invitrogen) and stimulated by indicated treatments. The cells were stained with Fixable Viability Dye or propidium iodide to label dead cells which were excluded in analysis. The stained cells were analyzed by Canto II flow cytometer (BD Biosciences) and data was analyzed using FlowJo software suite (Tree Star).

2.6. Enzyme-linked immunosorbent assays

The levels of interleukin-2 (IL-2), interleukin-4 (IL-4), interferon-γ (IFN-γ), and interleukin-17A (IL-17A) in the sera or cell culture supernatants were analyzed by ELISAs according to the manufacturer's instructions (Thermo Fisher Scientific Inc.). To determine the production of NP-specific antibodies, the serum was collected from NP-KLH or NP-LPS immunized mice at the stated time points. The 96 well clean flat bottom plates (Corning) were coated with 10 μg/ml NP_{32}-BSA (Biosearch Technologies) in PBS overnight at 4 °C. Plates were blocked in ELISA blocking buffer (50 mM Tris pH 7.5, 150 mM NaCl, and 1% BSA) for 1 hr at RT. Plates were washed for three times with wash buffer (0.05% Tween 20 in PBS). Sera were diluted according to optimization for each experiment in blocking buffer and incubated on the NP-BSA coated plate for 1 hr at RT. The plates were further washed and incubated with HRP-conjugated anti-mouse immunoglobulins (SBA Clonotyping System-HRP, Southern Biotech) for 1 hr at RT. The plates were then washed and the NP-bound antibodies were revealed by tetramethylbenzidine substrate (Clinical Science Products). Absorbance at 450 nm and 570 nm was measured with the Multiskan™ GO Microplate Spectrophotometer (Thermo Fisher Scientific Inc.).

2.7. NPGPx expression in SLE patients and healthy control

Twenty-four patients diagnosed with systemic lupus erythematosus (SLE) based on American College of Rheumatology criteria were referred to the Division of Rheumatology and Immunology at China Medical University Hospital (Taichung, Taiwan). Twelve healthy people were enrolled as controls. To determine the *NPGPx* gene expression in the peripheral blood mononuclear cells (PBMCs) from SLE patients or healthy controls, the PBMCs were resuspended in TriZol reagent and subjected to RNA extraction using Direct-zol™ RNA MiniPrep (Zymo Research). The RNA was reverse-transcripted into cDNA using Transcriptor First Strand cDNA Synthesis Kit (Roche Applied Science). The cDNA was subjected to the real-time PCR assay using the SYBR® FAST qPCR Kits (Kapa Biosystems) and StepOnePlus™ Real-Time PCR System (Thermo Fisher Scientific Inc.). For quantifying *NPGPx* gene expression in the PBMC samples, the cDNAs were subjected to Multiplex real-time PCR mRNA analysis using custom oligonucleotide primers and probes (Integrated DNA Technologies), iQ Multiplex Powermix (Bio-Rad), and a CFX96 Real-Time detection system (Bio-Rad). *GAPDH* served as an endogenous control to normalized the amount of sample cDNA. The primer and probe information were listed in Supplementary Table 1.

2.8. Immunoblotting and antibodies

Cells were washed with ice-cold PBS and lysed in a buffer containing 50 mM Tris pH7.4, 150 mM NaCl, 2 mM EDTA, 50 mM NaF, 0.1% SDS, 0.5% sodium deoxycholate, 1% NP-40, 0.1% Triton X-100, and protease and phosphatase inhibitor cocktail. Cell lysates were resolved by SDS-PAGE for immunoblotting with indicated antibodies and then detected with horseradish peroxidase-conjugated anti-rabbit or anti-mouse antibody (Jackson ImmunoResearch) or Clean-Blot IP detection Reagent (HRP) (Thermo) and chemiluminescent (ECL) reagent (Millipore). Antibodies against phospho-SLP76 (Tyr145) (EP2853Y) and phospho-VAV1 (Tyr174) (EP510Y) were purchased from Abcam. Antibodies against phospho-SRC (Tyr416) (#2101), phospho-ZAP70 (Tyr319) (#2717), phospho-ZAP70 (Tyr493) (#2704), ZAP70 (#3165), PLCγ1 (#5690), phospho-PLCγ1 (Tyr783) (#14008), phospho-LAT (Tyr191) (#3584), LAT (#9166), phosphor-SLP76 (Ser376)(#14745), SLP76 (#4958), PAK2 (#2608), phospho-ERK (Thr202/Tyr204) (#4370), ERK (#9102), phospho-IκB (Ser32/36) (#9246), IκB (#4814), phospho-Akt (Thr308) (#4056) and Akt (#9272) were purchased from Cell Signaling Technology. Antibodies against phospho-LAT (Tyr226) (#558363; BD Pharmingen), LCK (#610097; BD Pharmingen), HA.11 epitope tag (MMS-101P; Covance), VAV1 (GTX103489; Genetex), NPGPx (GTX108578; Genetex), GAPDH (GTX627408; Genetex), PDPK1 (17086-1-AP; Proteintech), phospho-CD3-ζ chain (Tyr142) (#558402; BD Pharmingen) CD3-ζ chain (sc-1239; Santa Cruz) and Flag tag (F3165; Sigma) were used. For generation of NPGPx-specific monoclonal antibody (7E7-3B2), recombinant NPGPx protein (19–187 a.a.) were used as immunogen to immunize Balb/c mice. The spleen cells from successful immunized mice were fused with myeloma cells to obtain antigen-specific hybridomas. The specificity of 7E7-3B2 monoclonal antibody was validated by using wild-type and *NPGPx*$^{-/-}$ MEFs or splenocytes (Supplementary Figs. 12A and 12B).

2.9. Plasmids

The full-length *ZAP70* and *VAV1* cDNAs were obtained from the cDNA of Jurkat T cells. The full length *NPGPx* cDNA was obtained from the pQXCIP-*hNPGPx* vector as previous described [31]. These genes were cloned into the pHE cloning vector using HE Swift Cloning kit (Tools). The Cys-to-Ser and Asp-to-Asn mutants of *ZAP70* and *NPGPx* were generated using PCR-based site-directed mutagenesis (Herculase II fusion DNA polymerase, Agilent) and confirmed by DNA sequencing. To generate 3X Flag-tagged *ZAP70* and *VAV1* expression constructs, *ZAP70* and *VAV1* cDNAs were subcloned from pHE vector into the p3XFlag-CMV-7.1-2 vector (Sigma-Aldrich, Inc.). To generate HA-tagged *VAV1* expression vector, *VAV1* cDNA was subcloned from pHE vector into the pcDNA3.0-HA vector (Addgene). WT and mutant *NPGPx* and 3X-Flag-*ZAP70* cDNAs were amplified through PCR and subcloned into pLAS5w.Pbsd-L-tRFP-C and pLAS3w.PeGFP-I2-Puro lentivira1l expression vector (National RNAi Core Facility, Taiwan), respectively. The pMD.G and pCMVΔR8.91 plasmids were obtained from National RNAi Core Facility, Taiwan for lentiviral preparation. The pET48-TEV-*hNPGPx* (amino acids 19–187) was constructed as previous described [31].

2.10. Co-immunoprecipitation (Co-IP)

Whole-cell lysates were prepared using a Nonidet™ P-40 (NP-40) lysis buffer (50 mM Tris-Cl (pH 8.0), 150 mM NaCl, 0.5% NP-40, protease and phosphatase inhibitor cocktails) followed by sonication and centrifugation at 12,000×g for 10 min at 4 °C. For Co-IP, 1 mg of the crude whole-cell extract was incubated with 1 μg target protein antibodies or control IgG at 4 °C for 2 h. Then, 50 μl prewashed protein A/G agarose (Thermo) were added to the mixture and incubated at 4 °C for additional 2 h with gentle agitation. For precipitation of HA- or Flag-tagged proteins, 20 μl anti-HA or M2 beads (Sigma), respectively, were used to precipitate target proteins from crude whole-cell extract. After extensive washing with a diluted NP-40 lysis buffer (0.1% NP-40), immunoprecipitated proteins were eluted with SDS sample buffer and analyzed by immunoblot.

2.11. Identification of NPGPx-interacting candidates involving in TCR signaling pathway

NPGPx-interacting proteins were immunoprecipitated from the crude whole-cell extract of anti-CD3 (5 μg/ml; OKT3)/anti-CD28 (1 μg/ml; CD28.2) co-stimulated NPGPx-expressed Jurkat T cells using NPGPx-specific monoclonal antibody (7E7-3B2). The immunoprecipitated samples were subjected to non-reducing SDS-PAGE analysis and the protein bands of interest were excised for in-gel digestion with trypsin, following analyzed by Orbitrap Elite™ Hybrid Ion Trap-Orbitrap Mass Spectrometer (Thermo Fisher Scientific Inc.). The identified NPGPx-interacting proteins were subjected to TCR signaling pathway analysis by Kyoto Encyclopedia of Genes and Genomes (KEGG) Expression Database (Kanehisa Laboratories).

2.12. Recombinant protein purification, in vitro protein interaction and mass spectrum analysis of disulfide bond interaction

The preparation of recombinant NPGPx WT and C2S2 (amino acids 19–187) were as described [31]. To prepare reduced or oxidized NPGPx, the proteins were treated with 10 mM Tris (2-carboxyethyl) phosphine (TCEP; Sigma) or 20 mM H_2O_2 (Sigma), respectively, for 1 hour at room temperature. TCEP and H_2O_2 were removed by buffer exchange using Amicon Ultra-10 (Millipore, Billerica, CA). For disulfide bond dependent complex analysis, 3XFlag-tagged ZAP70 or VAV1 were prepared from transduced 293T cells through immunoprecipitation by M2 beads (Sigma). The M2-bound purified proteins were incubated with 20 nM oxidized or reduced recombinant NPGPx at 25 °C for 1 h, following washed by wash buffer (50 mM Tris pH7.5, 450 mM NaCl, 0.5% NP-40, protease inhibitor cocktail) for 5 times. The beads were added with sample buffer without reducing agent and boiled at 95 °C for 10 min. The supernatant was separated on a 6% non-reducing SDS-PAGE gel, followed stained by InstantBlue (Expedeon). The protein bands of interest were excised for in-gel digestion with trypsin and chymotrypsin, following analyzed by tandem mass spectrometry. The MS/MS spectra were converted to the mgf format and analyzed by MassMatrix (http://www.massmatrix.net) to identify disulfide bonds as previously described procedures [31].

2.13. In vitro kinase assay

To perform *in vitro* kinases assays, the 3X Flag-ZAP70 WT or C/S mutant proteins were immunoprecipitated from transduced 293T cell lysates by anti-Flag M2 beads (Sigma) and competitively eluted by 100 μg/ml 3X Flag peptide (Sigma) in the TBS buffer containing 150 mM NaCl and 20 mM Tris (pH7.5) for 30 min at 4 °C. Eluted 3X Flag-ZAP70 protein was incubated with 15 or 30 μM oxidized NPGPx WT or C2S2 mutant in 20 μl TBS buffer for 1 hr at RT. The mixture was following incubated with immunoprecipitated HA-VAV1 beads from transduced HEK293T cells and reacted in 25 μl of the kinase buffer (25 mM Tris pH7.5, 10 mM $MgCl_2$, 100 μM Na_2VO_4, and 200 μM ATP) at 37 °C for 30 min. The reaction was stopped by the addition of Laemmli sample buffer and boiled at 95 °C for 10 min.

2.14. Immunofluorescent staining and microscopy

For the detection of ZAP70 distribution, 3xFlag-ZAP70 reconstituted P116 cells were stimulated and settled in the 0.01% poly-L-lysine precoated cover slide for 30 min at 4 °C, following fixed by 3.7% formaldehyde and permeabilized by 100 μg/ml digitonin for 10 min at RT each step. The slides were further blocked by 1% BSA for 30 min at RT and

incubated with goat anti-ECS(DDDDK) (A190-101A; Bethyl Laboratories, Inc.) to against the Flag-ZAP70 for 1 hr at RT. The slides were washed with 1% BSA containing 0.05% Triton-X100 for 10 min three times, following incubated with Alexa Fluor® 488 donkey anti-goat IgG (Invitrogen) for 1 hr at RT. After washed with washing buffer, the slides were counterstained with DAPI, and mounted using Fluorescent mounting medium (S3023, Dako). The cell images were captured by the SP5 confocal microscope (Leica Microsystems). The fluorescent intensity of the images was quantified using the ImageJ software. The relative intensity of Flag-ZAP70 in perimembrane region (0.5 μm on the periphery of the membrane) was normalized with the total fluorescent intensity of the cell.

2.15. In situ proximity ligation assay (PLA)

The stimulated cells were settled in the 0.01% poly-L-lysine precoated 8-well chamber slides (Millipore) for 30 min at 4 °C, following fixed by 3.7% formaldehyde and permeabilized by 100 μg/ml digitonin for 10 min at RT each step. The slides were further blocked by 1% BSA for 30 min at RT and incubated with primary antibodies (goat anti-ECS (DDDDK) (A190-101A; Bethyl Laboratories, Inc.), rabbit anti-NPGPx (GTX108578; Genetex), or rabbit anti-CD3ε (A0452; Dako)) for 1 hr at RT. The slides were washed with 1% BSA containing 0.05% Triton-X100 for 10 min three times, following incubated with PLA anti-Rabbit PLUS probe (Sigma) and PLA anti-Goat MINUS probe (Sigma) for 1 hr at 37 °C. The hybridization and ligation steps were performed using the Duolink® In Situ Fluorescent Detection Reagents (Sigma) according to the manufacturer's instructions. Afterwards, the slides were stained with DAPI and mounted with Fluorescence Mounting Medium (Dako), following analyzed by SP5 Confocal microscope (Leica Microsystems). PLA dot numbers were counted by ImageJ (National Institutes of Health). Over 150 cells were examined for each experiment.

2.16. Preparation of lipid raft fractions

The ZAP70 and NPGPx-reconstituted P116 cells were stimulated with 2 μg/ml anti-human CD3 (OKT3), following treated with 375 μg/ml of cold TNE buffer containing 0.05% Triton X-100, incubating for 30 min on ice. The TNE buffer is composed of 25 mM Tris (pH 7.5), 150 mM NaCl, 5 mM EDTA, 1X protease inhibitor, 1X phosphatase inhibitor. The lysates were then mixed with 375 μl 85% sucrose in TNE buffer. The mixture was over laid with 2.25 ml of 30% sucrose in TNE buffer, following by 1.5 ml of 5% sucrose in TNE buffer to generate the sucrose gradients. The sucrose gradients were covered by mineral oil and centrifuged at 200,000*g in a SW55Ti rotor (Beckman Coulter, Fullerton, CA) for 19 hours at 4 °C using Optimal™ L-90K Ultracentrifuge (Beckman Coulter, Fullerton, CA). Twelve fractions of proteins were added SDS sample buffer and resolved by SDS-PAGE and immunoblotting.

2.17. Statistical analysis

Data were presented as means ± SEM (for animal experiments analysis) or means ± SD (for cell line experiments) as indicated in figure legends, and data distribution was assumed to be normal. N number used in indicated section was shown in the figure legends. The difference of variance between the groups was statistically compared by F-test in all data. Most of the data were statistically compared by two-tailed unpaired Student's *t*-test when the two population variances were not significantly different. For the data that two population with unequal variance, two-tailed Welch's unequal variance *t*-test was used. Mann-Whitney nonparametric test was used to analyze the disease curve of EAE models. Statistical analyses were conducted using GraphPad Prism 5. Asterisk and indicate statistical significance with p-value < 0.05 (*), p-value < 0.01 (**), p-value < 0.001 (***), and p-value < 0.0001 (****).

3. Results

3.1. NPGPx and T cell-mediated immunity

We have previously reported that about 60% of the aged *NPGPx*$^{-/-}$ mice developed glomerulonephritis, splenomegaly, and lymphoma (Supplementary Figs. 1A–E) accompanied with immune complex deposition in the kidney [31]. In addition, these *NPGPx*$^{-/-}$ mice also developed elevated autoreactive anti-nuclear antibodies (ANAs), anti-dsDNA, and anti-ssDNA in the sera compared to the wild-type mice (Supplementary Figs. 1F–H), implicating that loss of NPGPx may lead to immune disorders. To explore how NPGPx participates in immune homeostasis, we first isolated different subsets of immune cells and

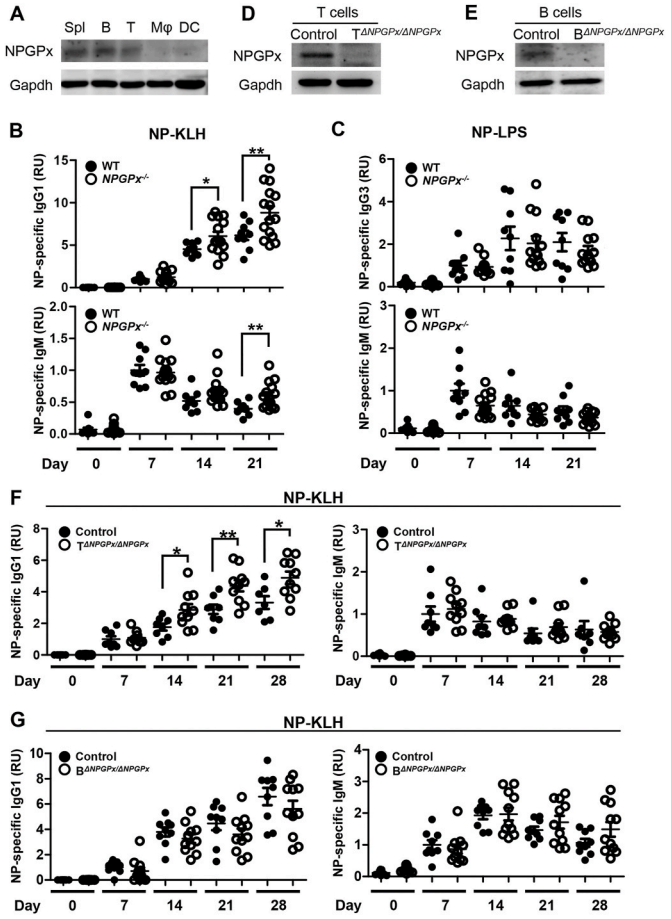

Fig. 1. NPGPx-deficiency leads to elevated T-dependent immune responses in mice.
(A) Western blotting analysis of NPGPx expression pattern in different hematopoietic lineages. Spl, spleen. Mφ, macrophages. DC, dendritic cells. **(B, C)** ELISAs of antigen-specific immunoglobulin productions in the sera from wild-type (WT, filled circles) or *NPGPx*$^{-/-}$ (open circles) mice after NP-KLH (**B**; WT, n = 9 mice; *NPGPx*$^{-/-}$, n = 15 mice) or NP-LPS (**C**; WT, n = 10 mice; *NPGPx*$^{-/-}$, n = 10 mice) immunization. RU, relative unit. **(D)** NPGPx expression in primary T cells from *NPGPx*$^{fx/fx}$ (Control) or *CD4-Cre; NPGPx*$^{fx/fx}$ (T$^{\Delta NPGPx/\Delta NPGPx}$) mice. **(E)** NPGPx expression in primary B cells from *NPGPx*$^{fx/fx}$ (Control) or *CD19-Cre; NPGPx*$^{fx/fx}$ (B$^{\Delta NPGPx/\Delta NPGPx}$) mice. **(F, G)** Control (n = 8 mice in **F**; n = 9 mice in **G**), T$^{\Delta NPGPx/\Delta NPGPx}$ (n = 10 mice), or B$^{\Delta NPGPx/\Delta NPGPx}$ (n = 11 mice) mice were immunized with NP-KLH. Levels of NP-specific IgG1 and IgM secretion in serum were determined by ELISAs. Data information: Experimental data were verified in three **(B, C)** or two **(F, G)** independent experiments with similar results. Values are mean ± SEM of biological replicates in **(B, C, F, G)**. Each sample was measured in technical triplicates. The mean values were used for statistical analysis. Level of significance was determined by two-tailed unpaired *t*-test, * = $p < 0.05$ and ** = $p < 0.01$.

determined that both T and B lymphoid cells expressed a higher amount of NPGPx (Fig. 1A and Supplementary Fig. 2) compared to the other immune cells. Interestingly, aged *NPGPx*$^{-/-}$ mice produced excessive IgG1 in the sera compared to the wild-type (Supplementary Fig. 1I). Since the induction of IgG1 class switching in B cells required T helper cell-mediated immune responses [40], we speculated that NPGPx might take a role in T-dependent humoral immunity. To test this possibility, we immunized wild-type and *NPGPx*$^{-/-}$ mice with T cell-dependent antigen

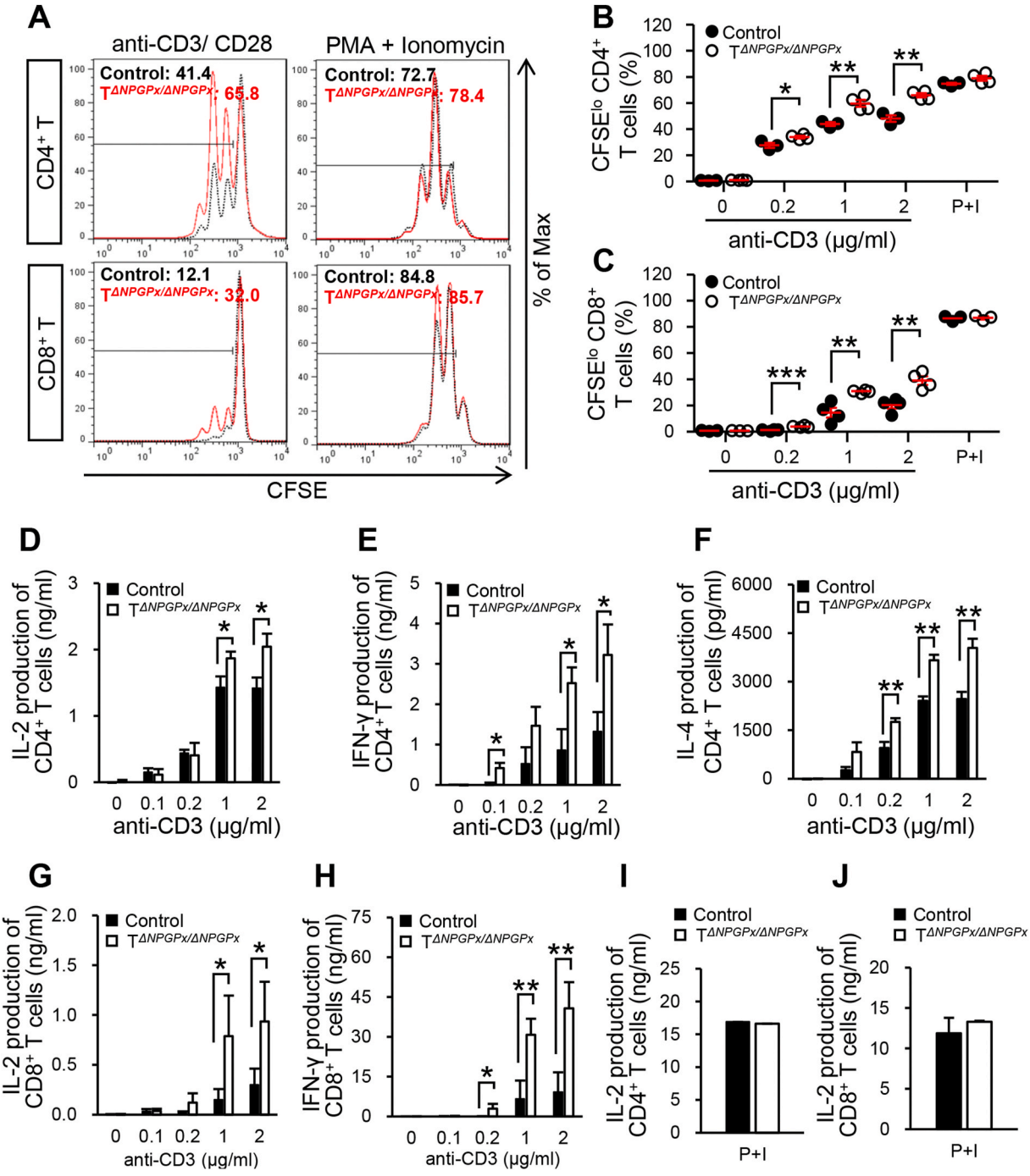

Fig. 2. T cell-intrinsic NPGPx deficiency contributes to T cell hyperactivation upon TCR stimulation.
(A) CFSE dilution assays of primary isolated CD4$^+$ or CD8$^+$ T cell proliferation at 48 h after anti-CD3 (1 μg/ml)/anti-CD28 (1 μg/ml) co-stimulation or PMA (50 ng/ml)/ionomycin (1 μM) co-treatment. **(B, C)** Frequency of divided CFSE (CFSE^{lo}) labeled CD4$^+$ T **(B)** or CD8$^+$ T cells **(C)** at 48 h after different concentration of anti-CD3 plus anti-CD28 (1 μg/ml) co-stimulation or PMA (50 ng/ml)/ionomycin (1 μM) treatment. Control, n = 3 or 4; T$^{\Delta NPGPx/\Delta NPGPx}$, n = 4. **(D–H)** ELISAs of cytokine levels in the culture supernatants from primary isolated CD4$^+$ T **(D–F)** or CD8$^+$ T **(G, H)** cells stimulated with different concentration of anti-CD3 plus anti-CD28 (1 μg/ml) co-stimulation. The culture supernatants were collected at 24 h (for IL-2 and IFN-γ productions) or 72 h (for IL-4 production) after stimulation. **(I, J)** ELISA of IL-2 level in the culture supernatants from primary control and T$^{\Delta NPGPx/\Delta NPGPx}$ mouse CD4$^+$ T **(I)** or CD8$^+$ T **(J)** cells stimulated with PMA (50 ng/ml)/ionomycin (1 μM) co-treatment for 24 h. Data information: Experimental data were verified in three independent experiments with similar results. Values are mean ± SEM of biological replicates in **(B, C)**, and mean ± SD of biological replicates in **(D–J)**. In **(D–J)**, each sample was measured in technical triplicates of ELISA. The mean values were used for statistical analysis. Level of significance was determined by two-tailed unpaired *t*-test, * = $p < 0.05$, ** = $p < 0.01$, and *** = $p < 0.001$.

(NP-KLH) or T cell-independent antigen (NP-LPS). After NP-KLH immunization, the serum from *NPGPx*$^{-/-}$ mice revealed higher levels of antigen-specific IgG1 compared to the wild-type mice (Fig. 1B). By contrast, when mice were immunized with NP-LPS, the serum levels of antigen-specific IgG3 and IgM were not elevated in *NPGPx*$^{-/-}$ mice (Fig. 1C).

To further validate whether NPGPx involves in the functions of T or B cells to promote T-dependent humoral responses, we generated the tissue-specific *NPGPx*-conditional knockout mice (Supplementary Fig. 3) and crossed with *CD4-Cre* transgenic mice [35] or *CD19-Cre* transgenic mice [41] to specifically deplete *NPGPx* expression in T (Fig. 1D) or B cells (Fig. 1E), respectively. The *CD4-Cre; NPGPx*$^{fx/fx}$ ($T^{\Delta NPGPx/\Delta NPGPx}$) and *CD19-Cre; NPGPx*$^{fx/fx}$ ($B^{\Delta NPGPx/\Delta NPGPx}$) mice were immunized with NP-KLH to examine their T-dependent humoral responses. We found that $T^{\Delta NPGPx/\Delta NPGPx}$ mice revealed elevated NP-specific IgG1 production (Fig. 1F), while that was comparable between $B^{\Delta NPGPx/\Delta NPGPx}$ and control (*NPGPx*$^{fx/fx}$) mice (Fig. 1G). In addition, loss of NPGPx in T cells did not affect T cell development (Supplementary Figs. 4A and B), and the FoxP3 levels and suppressive function of lymphoid tissues-derived regulatory T cells (Tregs) were also unaffected (Supplementary Figs. 4C and D), indicating the elevated T-dependent humoral responses in $T^{\Delta NPGPx/\Delta NPGPx}$ mice were not due to developmental disorders or impaired Treg functions. These results suggested that NPGPx takes a prominent role in modulating T cell functions to promote T-dependent immune responses.

To determine whether NPGPx modulates T cell activation, we isolated primary $CD4^+$ T or $CD8^+$ T cells from control and $T^{\Delta NPGPx/\Delta NPGPx}$ mice and induced T cell activation by TCR stimulation (anti-CD3 and anti-CD28 co-stimulation) or mitogenic stimulation (PMA and ionomycin co-treatment). Upon TCR stimulation, both $T^{\Delta NPGPx/\Delta NPGPx}$ $CD4^+$ and $CD8^+$ T cells showed a significant hyperproliferation (Fig. 2A–C and Supplementary Fig. 5) and elevated IL-2, IFN-γ, and IL-4 productions (Fig. 2D–H) compared to the wile-type cells. However, there was little difference in cell division and IL-2 production between control and $T^{\Delta NPGPx/\Delta NPGPx}$ $CD4^+$ or $CD8^+$ T cells upon mitogenic stimulation (Fig. 2A, I, and J), implicating that NPGPx may be involved in the TCR signaling-mediated T cell activation. The similar observations were also found in *NPGPx*$^{-/-}$ T cells (Supplementary Figs. 6A–J). Consistently, *NPGPx*$^{-/-}$ $CD4^+$ T cells show elevated expression of CD69 level upon TCR stimulation, but not mitogenic stimulation (Supplementary Fig. 6K). By contrast, neither anti-IgM antibodies nor anti-CD40/IL-4 co-stimulation revealed a difference in cell proliferation and IgG1-producing ability between wild-type and *NPGPx*$^{-/-}$ B cells (Supplementary Figs. 7A and B), suggesting that NPGPx does not contribute to BCR- or T cell-mediated activation in B cells. Taken together, these results provided evidences that NPGPx specifically involves in the negative regulation of TCR signaling module in T cells.

3.2. Exacerbated EAE in $T^{\Delta NPGPx/\Delta NPGPx}$ mice

T cells, especially T_H1 and T_H17 cells, serve a critical role in mediating the pathogenesis of EAE [42]. To examine the *in vivo* role of NPGPx in T cells, we immunized the control and $T^{\Delta NPGPx/\Delta NPGPx}$ mice with myelin oligodendrocyte peptide (MOG) to induce EAE. Indeed, $T^{\Delta NPGPx/\Delta NPGPx}$ mice developed severe EAE-diseased phenotypes (Fig. 3A). The titers of IFN-γ and IL-17A in sera were also significantly higher in $T^{\Delta NPGPx/\Delta NPGPx}$ mice compared to that in control mice (Fig. 3B and C). Also, the numbers of spinal cord infiltrating T_H1 and T_H17 cells were significantly increased in $T^{\Delta NPGPx/\Delta NPGPx}$ mice than in control mice at day 12 after immunization (Fig. 3D and E). To further examine how NPGPx-deficient $CD4^+$ T cells are activated upon antigen-specific stimulation, we re-stimulated the sensitized cells isolated from the draining lymph node of immunized mice with MOG peptides. MOG-re-stimulated $T^{\Delta NPGPx/\Delta NPGPx}$ cells revealed a higher percentage of dividing $CD4^+$ T cells (Fig. 3F) and more IFN-γ and IL-17A productions (Fig. 3G and H), indicating that the exacerbated EAE in $T^{\Delta NPGPx/\Delta NPGPx}$ mice was due to hyperactivation of antigen-specific T cells upon NPGPx deficiency. Furthermore, we also found the serum level of autoreactive ANAs was significantly enhanced in $T^{\Delta NPGPx/\Delta NPGPx}$ mice compared to the control mice in an age-dependent manner (Fig. 3I). These observations supported that T cell with intrinsic NPGPx deficiency gained T cell hyperactivation and promoted the humoral immune responses, provoking autoreactive antibodies productions. Interestingly, in human with SLE, whose serum autoreactive antibodies are usually elevated, *NPGPx* expression was low in T cells (Supplementary Fig. 8A; Data ref: GDS4719 [43]) [44]. By analyzing the PBMCs from 24 SLE patients and 12 age-matched healthy controls (Supplementary Table 2 and Supplementary Fig. 8B), we found that NPGPx expression levels were significantly lower in the PBMCs from SLE patients (Fig. 3J), and were not correlated with the age and the disease duration of these patients (Supplementary Figs. 8C and D). These results indicated that intrinsic *NPGPx* expression is required for T cell homeostasis to modulate the balance of T-dependent immune response.

3.3. NPGPx directly interacts with ZAP70 to modulate T cell responses

NPGPx serves as an oxidative stress sensor and deficiency of NPGPx results in ROS accumulation in several organs due to impaired chaperon activity and protein folding system [31,45,46]. To test whether ROS accumulation contributes the hyperactivation in NPGPx-deficient T cells during TCR stimulation, we measured the cellular ROS levels by oxidation-sensitive dye dichlorodihydro-fluorescein diacetate (DCFDA) labeling, and found that both the basal ROS levels and the kinetics of TCR-induced DCFDA oxidation were similar between *NPGPx*$^{-/-}$ and wild-type $CD4^+$ or $CD8^+$ T cells within 10 minutes (Supplementary Figs. 9A–D). However, NPGPx-deficiency resulted in the elevated ERK phosphorylation within this time point, indicating the exaggerated TCR signaling had occurred (Supplementary Fig. 9E). These results implicate an uncovered function of NPGPx in modulating TCR responses during early TCR stimulation.

It was noted that NPGPx regulates target protein functions through disulfide bond shuffling by its two redox-active cysteine residues, Cys57 and Cys86 [31,34]. Consistently, the sulfenylation of NPGPx, which is an intermediate step on the path toward NPGPx intramolecular disulfide bridge formation, was increased with TCR stimulation (Supplementary Fig. 10). To test whether the NPGPx-mediated redox regulatory mechanism occurred in T cells, we employed the NPGPx non-expressing Jurkat E6.1 T cells for expressing NPGPx WT (wild-type) or C2S2 mutant (C57S and C86S double mutant) through lentiviral transduction. It appeared that Jurkat E6.1 T cells ectopically expressing NPGPx WT, but not C2S2 mutant, reduced the IL-2 production upon TCR stimulation (Fig. 4A and Supplementary Fig. 11A). Similarly, Jurkat E6.1 T cells reconstituted with NPGPx WT showed lower CD69 expression compared to that of control and NPGPx C2S2 mutant transduced cells (Supplementary Fig. 11B), suggesting that the NPGPx-mediated disulfide bond shuffling plays an important role in response to TCR stimulation. Next, to explore how NPGPx modulates the TCR responses, we used immunoprecipitation coupled with mass spectrometry (IP–MS) to identify disulfide bond-dependent NPGPx-interacting target proteins (Supplementary Figs. 12A–D). These target proteins were subjected to the KEGG pathway analysis for their involvements in TCR signaling. Among these, the top five ranking of TCR signaling-related proteins, ZAP70, PDPK1, VAV1, PAK2, and AKT1, were identified (Supplementary Figs. 12E and F). Further validation by direct co-IP assay demonstrated that ZAP70 and VAV1 revealed 3.8 and 2-fold increases in association with NPGPx, respectively, after TCR stimulation for 15 minutes (Fig. 4B and C). By contrast, AKT1, PDPK1, and PAK2 displayed subtle increase or undetectable association with NPGPx upon TCR stimulation (Fig. 4B and C). To test whether ZAP70 or VAV1 interacts with NPGPx covalently, immunopurified Flag-ZAP70 or VAV1 from transduced 293T cells were incubated with H_2O_2-induced oxidized NPGPx (oxNPGPx) WT or C2S2 mutant, and subjected to non-reducing SDS-PAGE analysis (Fig. 4D). It

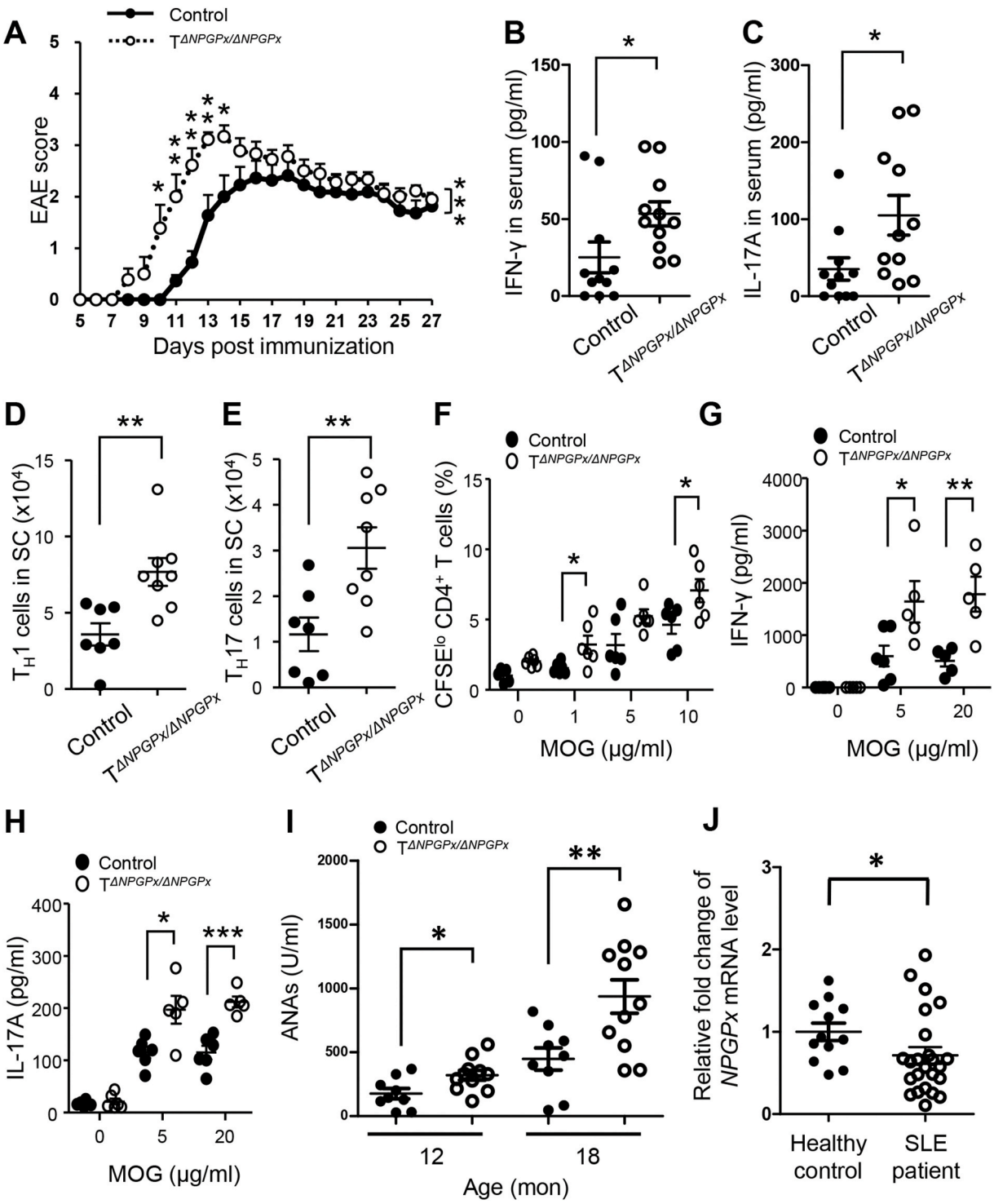

Fig. 3. T cell intrinsic NPGPx deficiency exacerbates EAE in mice.

(A) The EAE induction in control (n = 11 mice; filled circles) and $T^{\Delta NPGPx/\Delta NPGPx}$ (n = 9 mice; open circles) mice. Disease clinical scores (1–5) of mice are shown. Each data point represents the mean ± SEM of biological replicates. **(B, C)** ELISAs of IFN-γ (**B**) and IL-17A (**C**) levels in the sera from EAE-diseased mice at day 9. Control, n = 11 mice. $T^{\Delta NPGPx/\Delta NPGPx}$, n = 11 mice. **(D, E)** Cell numbers of infiltrating T_H1 **(D)** or T_H17 **(E)** cells in the spinal cords (SC) of EAE-diseased mice at day 12. Control, n = 7 mice. $T^{\Delta NPGPx/\Delta NPGPx}$, n = 8 mice. **(F)** Percentage of CFSE-labeled dividing cells isolated from the draining LNs of MOG-immunized mice after antigen restimulation for 120 h. Control, n = 6 mice. $T^{\Delta NPGPx/\Delta NPGPx}$, n = 6 mice. **(G, H)** ELISAs of IFN-γ **(G)** and IL-17A **(H)** levels in the culture supernatants from MOG-restimulated LN cells at 72 h n = 5 or 6 mice/group. **(I)** ELISA of anti-nuclear antibodies (ANAs) in the sera from 12- or 18-month-old mice. Control, n = 9 mice. $T^{\Delta NPGPx/\Delta NPGPx}$, n = 10 mice. **(J)** Expression of *NPGPx* mRNAs in PBMCs from SLE patients (n = 24 people) and healthy controls (n = 12 people) were determined by RT-qPCR. PBMC samples were obtained from CMUH in Taiwan. The *NPGPx* expression were normalized with *GAPDH* expression. Data information: Experimental data were verified in three **(A–E)** or two **(F–H)** independent experiments with similar results. Values are mean ± SEM of biological replicates. In (B, C, G, and H), each sample was measured in technical triplicates of ELISA. The mean values were used for statistical analysis. Level of significance was determined by two-tailed unpaired *t*-test, * = $p < 0.05$, ** = $p < 0.01$, and *** = $p < 0.001$. Mann-Whitney nonparametric test was used to analyze the significant difference between disease curves of EAE model in **(A)**, *** = $p < 0.001$.

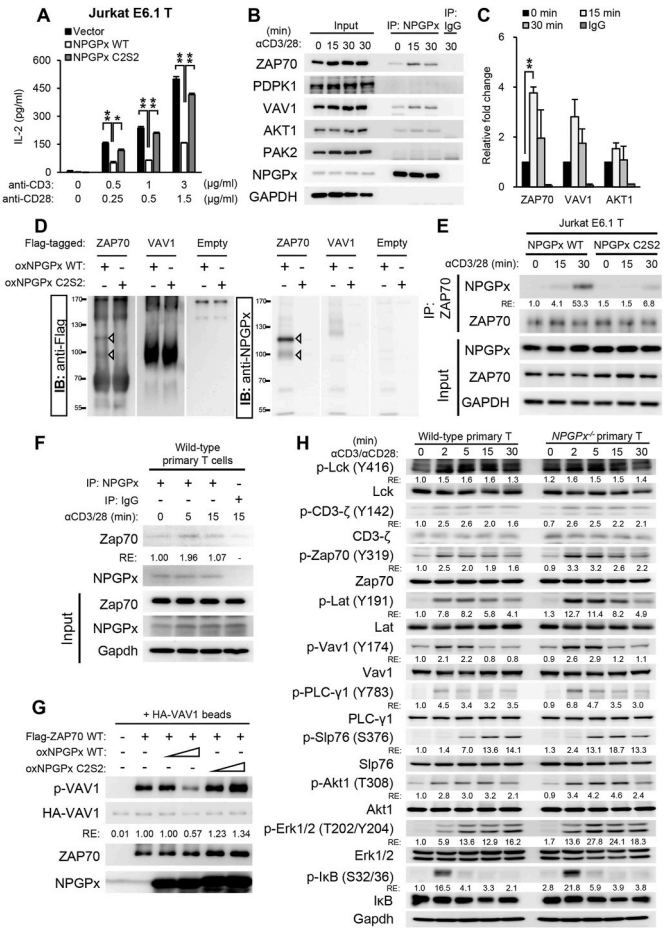

(caption on next column)

Fig. 4. NPGPx covalently interacts with ZAP70 to suppress its activity for modulating TCR responses.

(A) ELISA of IL-2 level in the culture supernatants from NPGPx WT or C2S2-expressing Jurkat E6.1 T cells stimulated with anti-CD3/anti-CD28 co-stimulation plus PMA (250 ng/ml) treatment for 24 h. **(B)** Co-IP of NPGPx in lysates prepared from NPGPx WT-expressing Jurkat E6.1 T cells with anti-CD3 (5 μg/ml)/anti-CD28 (1 μg/ml) co-stimulation for indicated time points. **(C)** The relative enrichment of the association of NPGPx and its interacting candidates after TCR stimulation quantified by spot densitometry according to **(B)**. **(D)** *In vitro* disulfide-bonded complex formation assay. The reaction mixtures containing H_2O_2-induced oxidized NPGPx WT or C2S2 recombinant proteins with M2-beads pull-down Flag-ZAP70 or Flag-VAV1 from 293T cells were separated by SDS-PAGE under non-reducing condition, and followed by western blotting. Disulfide bond-dependent complexes of NPGPx and ZAP70 were indicated by arrows. **(E)** Reciprocal co-IP of ZAP70 in lysates prepared from NPGPx WT or C2S2-expressing Jurkat E6.1 T cells with anti-CD3 (5 μg/ml)/anti-CD28 (1 μg/ml) co-stimulation for indicated time points. **(F)** Co-IP assay with anti-NPGPx showing the association of NPGPx and Zap70 was increased upon TCR stimulation. The primary T cells isolated from the wild-type or *NPGPx*$^{-/-}$ mice were stimulated with 10 μg/ml anti-CD3 plus 2 μg/ml anti-CD28 for indicated time periods. The cell lysates were used for IP with anti-NPGPx, following western blotting. **(G)** *In vitro* ZAP70 kinase assay. Immunopurified Flag-ZAP70 WT proteins were pre-incubated with H_2O_2-induced oxidized NPGPx WT or C2S2 proteins at room temperature for 1 h. The mixtures were following incubated with immunoprecipitated HA-VAV1 beads and subjected to immunoblotting analysis to examine VAV1 phosphorylation as the indicator of ZAP70 kinase activity. **(H)** Immunoblottings for TCR signaling molecules in primary T cells from wild-type or *NPGPx*$^{-/-}$mice with anti-CD3 (20 μg/ml)/anti-CD28 (5 μg/ml) co-stimulation. Data information: Experimental data were verified in three **(A, B, D, G, and H)** or two **(E, F)** independent experiments with similar results. Values are mean ± SD of technical triplicate measurement in **(A)** and of biological replicates in **(C)**. Level of significance was determined by two-tailed unpaired *t*-test, * = $P < 0.05$ and ** = $P < 0.01$. In **(E, F, G, and H)**, the intensity of each band was quantified using the ImageJ software. Relative enrichment of the association of NPGPx and Zap70 after TCR stimulation quantified in **(E and F)**. Total target protein expression was used as a control in **(G and H)**. Relative expression (RE) of protein levels in each figure is indicated.

was noticed that ZAP70 formed a significant amount of high-molecular weighted covalent complex with oxNPGPx WT, while VAV1 only had a weak complex formation with that (Fig. 4D). Moreover, the co-IP of NPGPx-ZAP70 was significantly reduced in cells expressing C2S2 mutant, supporting that NPGPx-ZAP70 interaction was mainly through covalently binding (Fig. 4E). This observation was further confirmed using murine primary T cells (Fig. 4F). Coincidentally, ZAP70 is the key tyrosine kinase for initiating the canonical TCR signaling pathways [20], but not VAV1. Thus, the interplay between NPGPx and ZAP70 should be of significance in this signaling pathway.

To explore whether NPGPx regulates the enzymatic activity of ZAP70, we performed an *in vitro* ZAP70 kinase assay through using VAV1 as the substrate. The phosphorylation ability of ZAP70 was suppressed after pre-incubated with oxNPGPx WT, but not C2S2 mutant (Fig. 4G), implicating that oxidized NPGPx binds to ZAP70 and functions as a negative regulator to inactivate ZAP70. A similar result was also obtained by using LAT as substrate in the assay (Supplementary Fig. 13). Moreover, the phosphorylation of ZAP70 and its downstream proteins, but not its upstream Lck and CD3-ζ chain, were all upregulated in *NPGPx*$^{-/-}$ T cells compared to wild-type T cells after TCR stimulation (Fig. 4H), supporting that NPGPx-deficiency leads to elevated ZAP70 activity in T cell. To further validate whether NPGPx regulates T cell responses through ZAP70 directly, we reconstituted both ZAP70 and NPGPx WT or C2S2 mutant into P116 cells, the ZAP70-deficient Jurkat T cell subclone, and found that the TCR-induced IL-2 production was suppressed only when P116 cells co-expressed with ZAP70 and NPGPx WT (Supplementary Figs. 11C and D). Taken together, these results suggest that NPGPx interacts with ZAP70 via disulfide bonding to negatively modulate ZAP70 kinase activity upon TCR stimulation.

3.4. Cys575 and Cys39 of ZAP70 are critical for NPGPx-mediated redox switching during TCR activation

Based on the above data and NPGPx functions as a redox sensor in signaling transmission [31], it should be of interest to explore the detail mechanism of how NPGPx regulates ZAP70 functions through redox switching. We first determined which cysteine residue (Cys, C) of ZAP70 forms covalent bonding with NPGPx by analyzing the NPGPx-ZAP70 complex from non-reducing SDS-PAGE with mass spectrometry (Fig. 5A), and found that four cysteine residues of ZAP70, Cys39, Cys84, Cys560, and Cys575, inclined to form intermolecular disulfide bonds with NPGPx (Fig. 5B). Next, we examined which cysteine residue involves in NPGPx-mediated ZAP70 kinase activity by using serine (Ser, S) substitutions at the indicated cysteine residues. The inhibitory effect of oxNPGPx WT to ZAP70 kinase activity was observed in this assay, but abolished when ZAP70 WT was replaced with ZAP70 C39S (Fig. 5C). However, ZAP70 C84S or C560S mutants behaved like ZAP70 WT, while C575S mutant appeared to be kinase-dead (Fig. 5C). In addition, oxNPGPx WT suppressed the kinase activity of ZAP70 WT, but not ZAP70 C39S mutant, in a dose-dependent manner (Fig. 5D), suggesting that Cys39 of ZAP70 was one of the key residues involving in the NPGPx-ZAP70 interplay. To test whether Cys39 or Cys575 of ZAP70 is required for the direct disulfide bonding between NPGPx and ZAP70, we performed non-reducing SDS-PAGE assay for detecting the higher molecular-weight complex. As shown in Fig. 5E, the covalent NPGPx-ZAP70 complexes were observed in ZAP70 WT and significantly elevated when ZAP70 C39S was used, implicating that a substitution of Cys39 to serine resulted in trapping ZAP70 on NPGPx. Interestingly, the complexes were not formed when ZAP70 C575S and C2S2 (C39S and C575S double mutant) were used (Fig. 5E). Based on these results, it is likely that Cys575 of ZAP70 could be the first residue targeted by NPGPx, while Cys39 of ZAP70 contributes to completing the NPGPx-mediated inhibition of ZAP70 activity.

To examine the biological significance of Cys39 and Cys575 in ZAP70, we transduced WT or mutants of C575S, C39S, and C2S2 (combined C39S and C575S) into P116 cells. The expression of NPGPx suppressed the TCR-induced IL-2 production in ZAP70 WT-reconstituted P116 cells, while this inhibitory effect was abrogated in ZAP70 C39S mutant cells (Fig. 5F), supporting that the Cys39 of ZAP70 is crucial for NPGPx-mediated regulation in ZAP70 activity. Notably, previous studies have already indicated the importance of Cys575 in regulating the stability and activity of ZAP70 [47]. Consistently, it was also found that ZAP70 with a substitution in Cys575 had no detectable kinase activity (Fig. 5C) and reduced protein expression due to its instability (Supplementary Figs. 14A and B), in spite of normal mRNA expression (Supplementary Fig. 14C). Thus, P116 cells reconstituted with ZAP70 C575S produced very low level of IL-2 upon TCR stimulation, similar to that in the P116 cells reconstituted with kinase-dead ZAP70 D461 N (Fig. 5F). Interestingly, unlike the ZAP70 WT required TCR stimulation to promote its association with NPGPx, ZAP70 C39S inclined to associate with NPGPx even at resting stage in reconstituted P116 cells (Fig. 5G). By contrast, the association with NPGPx was undetectable in ZAP70 C575S or C2S2 (combined C39S and C575S) mutants upon TCR stimulation in spite of five-fold more cell lysates were used to minimize the protein instability effect of ZAP70 Cys575 mutant (Fig. 5G). Taken together, these results suggested that Cys575 of ZAP70 is crucial for the initiation of its disulfide bonding with NPGPx and both Cys575 and Cys39 are required for the redox switching between NPGPx and ZAP70 upon TCR activation.

3.5. NPGPx reduces cytosolic ZAP70 to associate with TCR/CD3 complex at membrane lipid rafts

According to the above data, the interaction between NPGPx and ZAP70 was clearly established. However, the detailed mechanistic steps about how NPGPx negatively modulates ZAP70 during TCR stimulation in cells remain to be elucidated. It was noted that T cell activation requires the translocation of ZAP70 from the cytoplasm to the TCR stimulation-induced lipid raft microdomains in the plasma membrane for signaling transduction [48,49]. Since the Cys39 of ZAP70 is located in the SH2 domains, which required for its CD3-ITAM binding to mediate ZAP70 translocation, it was likely that NPGPx takes a role during this process. To explore whether NPGPx affects the translocation of ZAP70, we traced ZAP70 distribution in ZAP70-reconstituted P116 cells expressing either NPGPx or not. In ZAP70-reconstituted P116 control cells, ZAP70 was located diffusely throughout the cytoplasm in resting stage. After TCR stimulation by adding anti-CD3, ZAP70 translocated from cytosol to membrane and formed the microdomain clustering (Fig. 6A). However, expressing NPGPx reduced ZAP70 at the membrane microdomains upon anti-CD3 stimulation (Fig. 6A). Consistently, the quantitative data showed that NPGPx-expressing cells had a significantly less ZAP70 localized at the perimembrane region than that of control cells upon anti-CD3 stimulation (Fig. 6B). By using co-IP assay, we also observed that the TCR-induced association of ZAP70 and CD3-ζ chain, which containing the docking sites for ZAP recruitment to membrane TCR/CD3 complex, was reduced in NPGPx-expressing cells compared to that of the control cells (Fig. 6C). Conversely, ZAP70 recruitment to the CD3-ζ chain was elevated in TCR-induced NPGPx-deficient T cells (Fig. 6D), supporting that NPGPx reduces ZAP70 recruitment to TCR/CD3 complex upon TCR stimulation.

To further validate this observation, we performed sucrose gradient experiments to physically separate lipid rafts for examination of the TCR stimulation-induced redistribution of ZAP70. As shown in Fig. 7A, ZAP70 WT was recruited to lipid rafts within 5 min after TCR stimulation, while much less lipid raft-associated ZAP70 WT was found in NPGPx WT-expressing cells comparing to the control cells. Consistently, in the NPGPx C2S2-expressing cells, the reduction of ZAP70 WT in the raft fraction was not observed (Supplementary Fig. 15A). Furthermore, we performed the co-IP assay with anti-CD3-ζ chain antibodies, and found that the association of ZAP70 WT with CD3-ζ chain was reduced in NPGPx WT, but not C2S2 mutant, expressing cells following TCR stimulation (Supplementary Fig. 15B). On the other hand, despite the mutation of Cys39 intrinsically reduced ZAP70 ability in association with CD3-ζ chain, expressing NPGPx WT could not further diminish the association of ZAP70 C39S with raft-located CD3-ζ chain than that of ZAP70 WT following TCR stimulation (Fig. 7B and C), indicating that the Cys39 of ZAP70 is important for NPGPx-mediated modulation in ZAP70 recruitment to TCR/CD3 complex. Taken together, these results suggest that the disulfide bond shuffling between ZAP70 and NPGPx is involved in early TCR response.

To strengthen the above observations in cells, we performed proximity ligation assay (PLA) to show the translocation of ZAP70 and its colocalization with the cytosolic domain of CD3ε. Upon TCR stimulation with anti-CD3, the numbers of CD3ε-ZAP70 PLA signal dots were increased significantly in control ZAP70 WT cells, while this increase was not observed when NPGPx was expressed (Fig. 7D and Supplementary Fig. 16A). However, when ZAP70 Cys39 was mutated, the CD3ε-ZAP70 PLA signals were dramatically reduced regardless of the presence of NPGPx WT (Fig. 7D and Supplementary Fig. 16A). On the other hand, the NPGPx-ZAP70 interactions were prompted by anti-CD3 stimulation in NPGPx-expressed ZAP70 WT cells, while these interactions were elevated even in resting stage when the Cys39 of ZAP70 was mutated, and persisted highly after anti-CD3 stimulation (Fig. 7E and Supplementary Fig. 16B). These results indicate that NPGPx negatively regulates TCR stimulation-induced redistribution of ZAP70 through disulfide bond shuffling.

To further address whether the NPGPx-mediated restriction of ZAP70 recruitment to TCR/CD3 complex affects the signal transmission, we examined the phosphorylation of ZAP70 and its downstream molecules upon TCR stimulation. Expression of NPGPx suppressed the phosphorylation of ZAP70 at Y493 and its downstream molecules in ZAP70 WT reconstituted cells, while these phosphorylations were

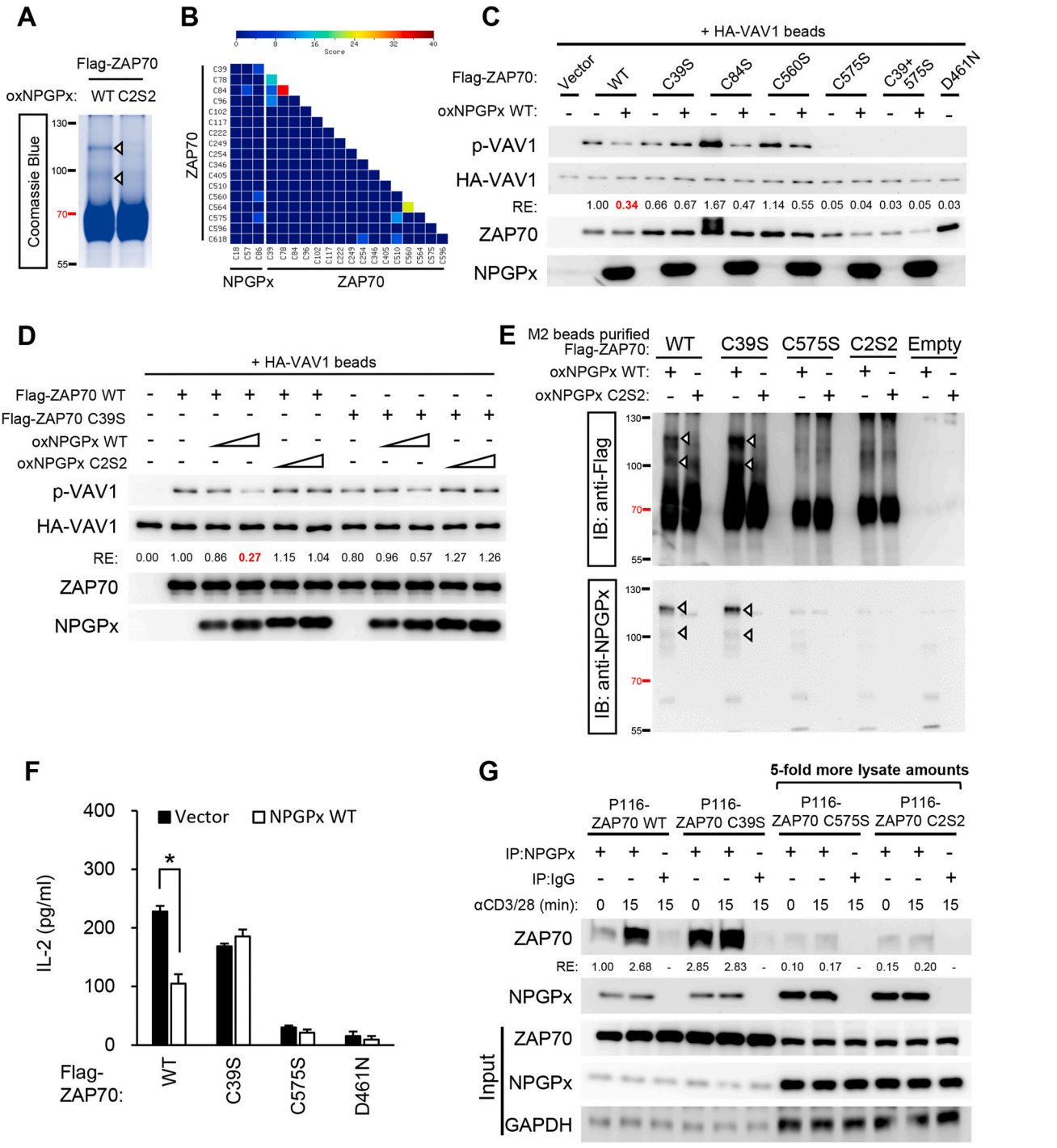

Fig. 5. The Cys39 and Cys575 of ZAP70 are required for NPGPx-mediated modulation during TCR stimulation.
(A, B) Identification of the intermolecular disulfide bonds between NPGPx and ZAP70. **(A)** Disulfide-linked complexes of NPGPx and ZAP70 were separated by SDS-PAGE under non-reducing condition and indicated by arrows. **(B)** Identification of inter- and intra-molecular disulfide bonds within ZAP70 and NPGPx by mass spectrometry analysis. **(C, D)** *In vitro* ZAP70 kinase activity to examine the inhibitory efficiency of H_2O_2-induced oxidized NPGPx (oxNPGPx) WT to ZAP70 WT or C/S mutants. The relative enzymatic activity of ZAP70 in complexed with oxNPGPx WT was labeled in red. **(E)** *In vitro* disulfide-bonded complex formation assay. Immunopurified Flag-ZAP70 WT or C/S mutants from 293T cells were incubated with H_2O_2-induced oxidized NPGPx WT or C2S2 recombinant proteins, and subjected to non-reducing SDS-PAGE analysis to examine the intermolecular disulfide bond-dependent complexes indicated by arrows. **(F)** ELISA of IL-2 level in the culture supernatants from ZAP70 and NPGPx reconstituted P116 cells stimulated with anti-CD3 (10 μg/ml)/anti-CD28 (5 μg/ml) co-stimulation plus PMA (250 ng/ml) treatment for 24 h **(F)**. **(G)** Co-IP of NPGPx in lysates prepared from ZAP70 and NPGPx reconstituted P116 cells with anti-CD3 (10 μg/ml)/anti-CD28 (2 μg/ml) co-stimulation. Data information: Experimental data were verified in three independent experiments with similar results. Values are mean ± SD of technical triplicate measurement in **(F)**. Level of significance was determined by two-tailed unpaired *t*-test, * = $P < 0.05$. In **(C, D, and G)**, the intensity of each band was quantified using the ImageJ software. HA-VAV1 expression was used as a control to examine p-VAV1 expression in **(C and D)**. Relative enrichment of the association of NPGPx and ZAP70 after TCR stimulation quantified in **(G)**. Relative expression (RE) of protein levels in each figure is indicated. (For interpretation of the references to colour in this figure legend, the reader is referred to the Web version of this article.)

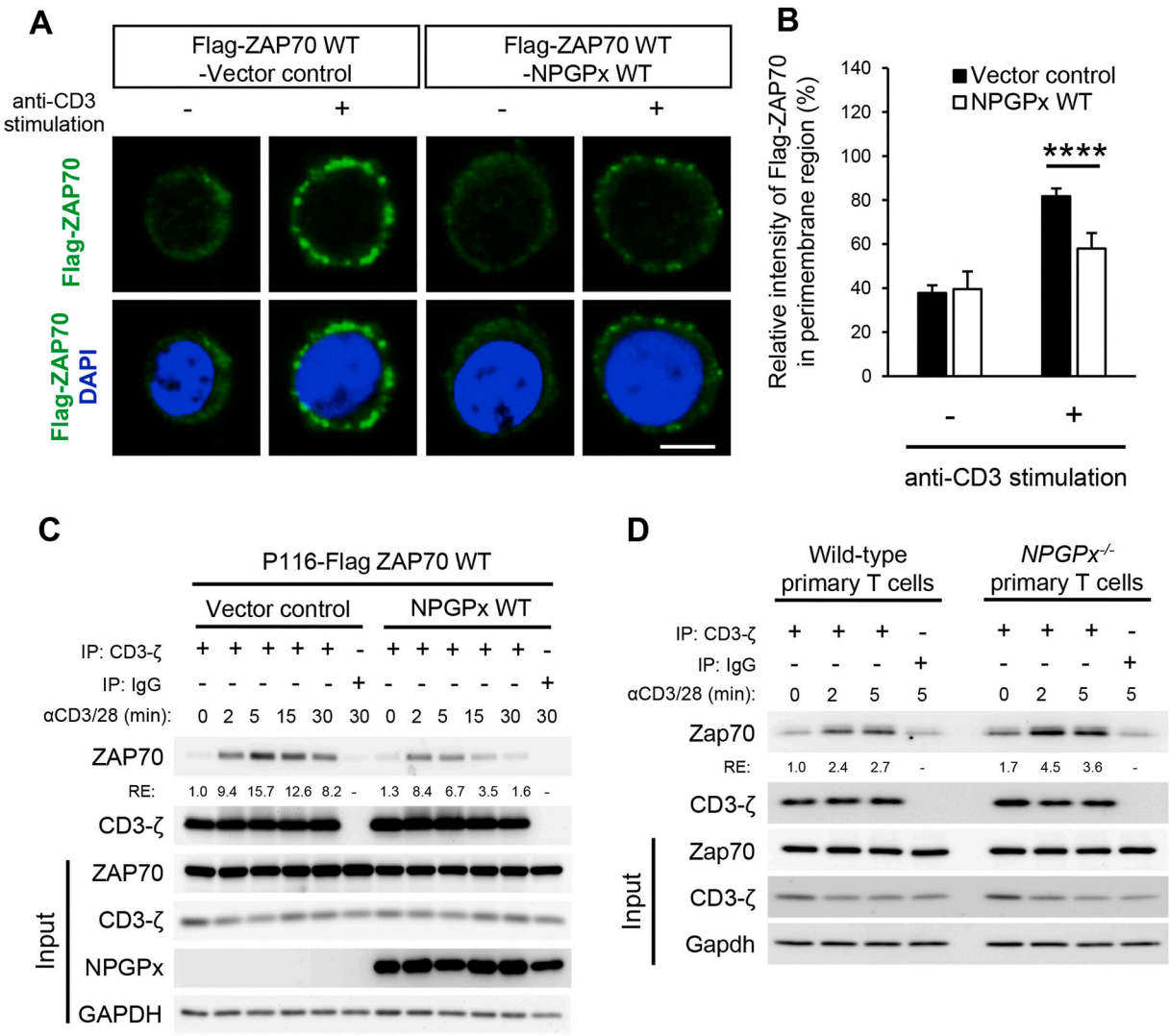

Fig. 6. NPGPx reduces ZAP70 translocation to bind TCR/CD3 complex upon TCR stimulation.
(A) IF staining to demonstrate the cellular distribution of ZAP70 upon TCR stimulation. Flag-tagged ZAP70 WT reconstituted P116 cells combined NPGPx WT expression or vector control were stimulated with anti-CD3 (1 μg/ml) for 5 min. Cells were fixed and processed for IF staining with anti-Flag (Green) and DAPI (Blue). **(B)** Quantitative results show the percentage of relative Flag-ZAP70 fluorescent intensity in the perimembrane region. unstimulated vector control cells, n = 6; unstimulated NPGPx WT cells, n = 4; stimulated vector control cells, n = 9; Stimulated NPGPx WT cells, n = 8. ****$p < 0.0001$. Scale bar, 5 μm. **(C)** Association of ZAP70 and CD3-ζ chain by co-IP assay was decreased in NPGPx WT reconstituted cells. Co-IP of CD3-ζ chain in lysates prepared from ZAP70 WT and NPGPx WT reconstituted P116 cells treated with anti-CD3 (10 μg/ml) plus anti-CD28 (2 μg/ml) for indicated time periods. **(D)** *NPGPx* deficiency promotes the association of Zap70 and CD3-ζ chain. The primary T cells isolated from the spleen and lymph nodes of wild-type or *NPGPx*$^{-/-}$ mice were stimulated with 10 μg/ml anti-CD3 plus 2 μg/ml anti-CD28 for indicated time periods. The cell lysates were used for IP with anti-CD3-ζ, following subjected to western blotting. Relative enrichment of the association of ZAP70 and CD3-ζ chain after TCR stimulation quantified by spot densitometry. Data information: Experimental data were verified in three **(A, B)** or two **(C, D)** independent experiments with similar results. (For interpretation of the references to colour in this figure legend, the reader is referred to the Web version of this article.)

dramatically reduced when the Cys39 of ZAP70 was mutated regardless of the presence of NPGPx WT (Fig. 7F). Consistently, it was found that little or no association of NPGPx with phospho-Y493-ZAP70 was detected in NPGPx WT reconstituted Jurkat E6.1 T cells upon TCR stimulation (Supplementary Fig. 17). These results implicated that NPGPx-mediated redox responses contribute to less membrane translocation and consequentially lacking the conformational change of ZAP70 for LCK-mediated phosphorylation to provoke its activity, supporting the notion that NPGPx negatively regulates ZAP70 recruitment to raft-associated TCR/CD3 complex through disulfide bond shuffling to curb ZAP70 activity during early TCR response.

4. Discussion

Emerging evidences indicated that the functional redox machineries are imperative for maintaining intact T cell responses [8–10,14,15]. Redox changes can alter T cell proteome through oxidative thiol modification of redox-sensitive cysteine residues [50] and blocking of reversible cysteine sulfenic acid by dimedone treatment suppresses T cell responses [51], implicating that oxidative thiol modification of specific target proteins is critical for T cell functions. Despite the TCR-proximal kinases are crucial for the ROS production to fire up T cell activation [52], ROS may conversely affect the oxidative thiol modification of these TCR-proximal kinases to maintain T cell homeostasis. The discovery described herein that NPGPx, the oxidative stress sensor, regulates and restrains ZAP70 kinase activity during TCR activation,

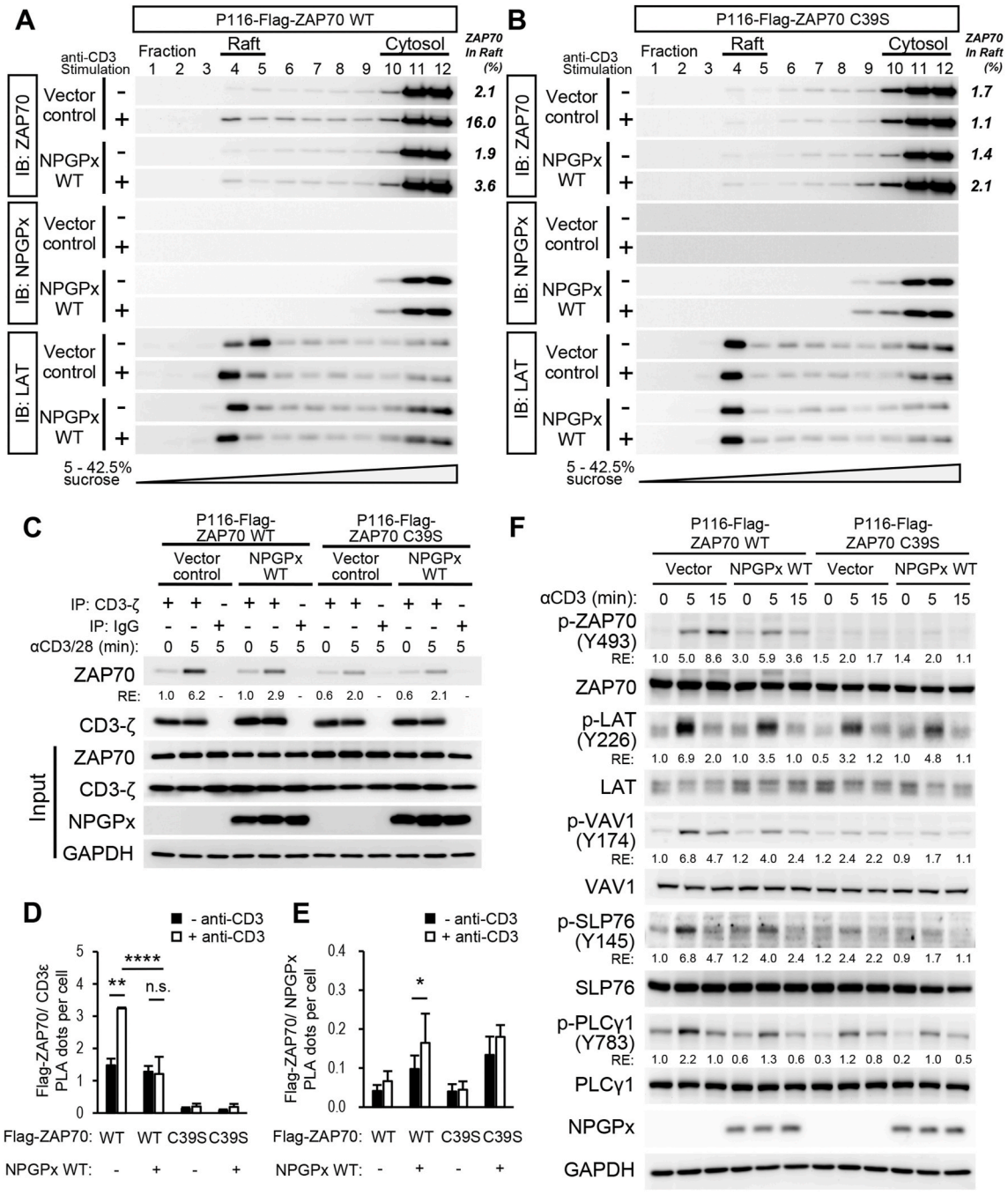

Fig. 7. NPGPx reduces ZAP70 to bind raft-associated TCR/CD3 complex for attenuating TCR responses.
(A, B) Flag-tagged ZAP70 WT **(A)** or C39S mutant **(B)** reconstituted P116 cells combined NPGPx WT expression or vector control were stimulated with anti-CD3 (2 μg/ml) for 5 min. The cell lysates were centrifuged by sucrose gradient to isolate the lipid rafts. Fractions were collected from top to bottom and analyzed by SDS-PAGE and immunoblotted with anti-ZAP70, anti-NPGPx, and anti-LAT. **(C)** Co-IP assay showing the association of ZAP70 WT, but not C39S, with CD3-ζ chain was decreased in NPGPx WT reconstituted cells. Co-IP of CD3-ζ chain in lysates prepared from ZAP70 WT and NPGPx WT or C2S2 reconstituted P116 cells treated with anti-CD3 (10 μg/ml) plus anti-CD28 (2 μg/ml) for indicated time periods. **(D, E)** Quantitation of the PLA signal dots of Flag-tagged ZAP70 with CD3ε **(D)** or NPGPx **(E)** upon anti-CD3 (1 μg/ml) stimulation for 5 min. More than 200 cells were analyzed and PLA dots were quantitated by ImageJ software. **(H)** Immunoblotting of proximal TCR signaling molecules in the lysates from ZAP70 and NPGPx reconstituted P116 cells after anti-CD3 (1 μg/ml) stimulation. Data information: Experimental data were verified in three independent experiments with similar results. Values are mean ± SD. Level of significance was determined by two-tailed unpaired *t*-test, * = $p < 0.05$, ** = $p < 0.01$, and **** = $p < 0.0001$. n.s., nonsignificant. In **(A, B, C, and F)**, the intensity of each band was quantified using the ImageJ software. Relative percentage of Flag-ZAP70 in raft was indicated in **(A and B)**. Relative enrichment of the association of ZAP70 and CD3-ζ after TCR stimulation quantified in **(C)**. In **(F)**, Total target protein expression was used as a control. Relative expression (RE) of protein levels in each figure is indicated.

providing a clear evidence to support this notion. Based on the above data and general redox reaction mode [31], we postulated the potential molecular mechanism as follows: after peptide-MHC and TCR engagement, cytosolic ZAP70 is recruited to the membrane lipid rafts by p-ITAMs and activated by LCK, initiating TCR signaling cascades and ROS production to provoke T cell activity. In response to the produced ROS, NPGPx senses it and forms intramolecular disulfide bonding between Cys57 and Cys86, further transferring the oxidative signal to

Cys575 and Cys39 of ZAP70, and NPGPx is released for recycling. The oxidized ZAP70 may be retained in cytosol and could not be recruited to the TCR/CD3 complex. Thus, NPGPx prevents T cell hyperactivation (Fig. 8A). Conversely, without NPGPx, the TCR-induced translocation of ZAP70 to TCR/CD3 complex in lipid rafts is not restrained, resulting in elevated TCR responses and T cell hyperactivation (Fig. 8B). This model provided a delicate redox mechanism mediated by NPGPx to fine-tune ZAP70 functions in maintaining T cell homeostasis and preventing immune disorders.

It was noted that ZAP70 plays a key role in T cell activation [20,21] and biochemical modifications such as ubiquitination and dephosphorylation modulating ZAP70 activity have an important role in TCR responses and T cell homeostasis [53–55]. Beyond these modifications, a novel redox regulatory mechanism of ZAP70 by NPGPx, as described herein, highlights the intimate link between oxidative modulation and TCR responses. Interestingly, the Cys39 and Cys575 of ZAP70 are crucial for NPGPx-mediated disulfide bond shuffling in response to ROS generated by TCR stimulation. ZAP70 C575S mutant fails to associate with NPGPx, while ZAP70 C39S mutant inclines to trap on NPGPx at the resting state but is unable to be recruited to the TCR/CD3 complex in lipid raft upon TCR stimulation. Based on these results, it is reasonable to deduce that oxidized NPGPx triggered by TCR activation may transfer the signal to ZAP70 through disulfide bond shuffling, in turn retaining ZAP70 in the cytosol to curb TCR responses. Consistently, it is noted that Cys39 locates at the SH2 domain and its oxidative modification suppresses the ITAM binding ability of ZAP70 [56]. The crucial role of Cys575 in ZAP70 stability and activity also has been mentioned as it located at a highly conserved redox-active $Mx_{(2)}CWx_{(6)}R$ motif in the kinase domain [30,47]. Other protein tyrosine kinases (PTKs) also have been found that mutation of the redox-sensitive cysteine residue located in this motif, such as Cys498 of SRC, Cys506 of YES, Cys475 of LCK, and Cys479 of LYN, contributes to impaired catalytic activity and in some case also protein instability [57–59]. One might be expected that other PTKs are also regulated by similar redox process as the described herein. Accordingly, our results illuminate the imperative roles of NPGPx-mediated redox regulation in ZAP70 biological functions through modulating specific cysteine residues. It has been reported that a dramatic conformational change by forming intramolecular disulfide bonding was found in several redox-regulated proteins in oxidative state such as Yap1 [60], ERO1 [61], and KEAP1 [62]. Therefore, how disulfide bond shuffling promotes conformational changes of ZAP70 affecting its physiological role could be of interest to further pursue.

The thiol-based redox regulatory mechanism of NPGPx is different from other GPx homologs that use GSH as a cofactor to detoxify cellular oxidative stress. Unlike GPx1 and GPx4 mediate T cell functions through directly scavenging ROS [63,64], NPGPx takes roles in T cell biological contexts by serving as a redox sensor/transmitter to modulate ZAP70 activity. In supporting this notion, Zap70-dependent signaling was hyperactive in NPGPx-deficient T cells compared to wild-type T cells (Fig. 4H), leading to higher cell proliferation and cytokine productions (Fig. 2A–H) when treated with anti-CD3/28 to induce TCR response. Comparable cell proliferative rate and IL-2 production were observed between wild-type and NPGPx-deficient T cells when treated with mitogen to directly evoke Ca^{2+}-dependent ROS production (Fig. 2A–C, I, and J). Furthermore, upregulation of Zap70 and its downstream substrates was observed in NPGPx-deficient T cells within 15 minutes after TCR stimulation when compared with the wild-type cells (Fig. 4H), while the ROS level was comparable between these two cell types at this time point (Supplementary Figs. 9A–D). Importantly, only NPGPx WT, but not C2S2 mutant, reduces ZAP70 association with CD3-ζ chain at lipid raft within 5 minutes after TCR stimulation (Fig. 6C and Supplementary Fig. 15). Consistently, the Cys39 and Cys575 of ZAP70 are critical for the ZAP70-NPGPx redox switching as we observed that the suppressive effect of NPGPx in ZAP70 recruitment to TCR/CD3 complex was abolished in ZAP70 C39S mutant cells (Fig. 7). Since the redox status in the cell maintains homeostasis in the steady state, it could be deduced that NPGPx also senses the regional ROS signal and forms complex with ZAP70 at the resting state. Interestingly, we found that sulfenylated NPGPx (Supplementary Fig. 9) and NPGPx-ZAP70 complex (Fig. 4B) exist at the steady state, and increase with TCR stimulation. ZAP70 C39S inclines to associate with NPGPx even at resting stage in reconstituted P116 cells (Fig. 5G), and the dissociation of the NPGPx-ZAP70 complex is prevented due to the Cys39 mutation of ZAP70. These results suggest a potential role of NPGPx in maintaining the resting state of naïve T cells. Another cysteine-containing GPx homolog in yeast, GPx3/Orp1, also functions as a redox-transducer in modulating the nuclear retention of transcriptional factor Yap1 through disulfide bond shuffling [65]. Interestingly, recent reports also showed that NPGPx and GPx8, which share similar amino acid sequence and protein structure, could negatively regulate OGA and caspase 4/11 enzymatic activity, respectively [66,67]. These observations infer the exceptional role of cysteine-containing GPxs in redox balance by switching the structure and activity of target proteins to modulate oxidative stress. It was noted that deficiency of NPGPx generates higher accumulated oxidative stress in later development through reducing GRP78 chaperon activity [31]. This effect should also be present in NPGPx-deficient T cells and the higher accumulated oxidative stress may affect biological functions of T cells. This possibility is interesting and worth further exploring.

Surprisingly, despite B cells express NPGPx, NPGPx deficiency does not affect the cell proliferation and antibody-producing ability (Fig. 1G and Supplementary Fig. 7). It was also noted that another GPx family membrane, GPx4, is important for T cell responses [64] but dispensable for conventional B cell (also called follicular B2 cell) functions [68]. Compared to the T cells, B2 cells are exposed to higher levels of ROS during development and activation and develop a more robust antioxidant system to adapt the redox changes [69]. Importantly, these antioxidant mechanisms have compensatory functions, which explain why the deficiency of GPx4 or thioredoxin-1 system shows limited effect B2 cell functions [68,70]. The deficiency of the NPGPx-mediated redox mechanism may be compensated by other redox mechanisms in B cells. Moreover, the Cys39 in ZAP70 is not conserved in spleen tyrosine kinase (Syk) [56], which is a ZAP70 homolog protein in B cell. The disulfide bond shuffling mediated by NPGPx should not be occurred in Syk. These could partially explain why NPGPx-deficiency does not affect B cell responses.

It was reported that either loss- or gain-of-ZAP70 functions in T cells provokes severe autoimmunity [71,72]. Likely, dysfunction of the fine-tune mechanism of ZAP70 could be the major cause for common autoimmune diseases. As described herein, mice with T cell-specific NPGPx deficiency display elevated T-dependent humoral immunity (Fig. 1F) and exacerbated EAE (Fig. 3A–H), indicating that loss of NPGPx-mediated ZAP70 negative regulation could increase the susceptibility of autoimmunity. Consistently, impairments of other negatively regulatory mechanisms of ZAP70, such as Nrpb1-mediated ubiquitination [55] and Sts1/2-mediated dephosphorylation [53], also led to T cell hyperactivation and severer EAE phenotypes in mice. Of note, the encephalitogenic Th1 and Th17 cells provoke the inflammatory and demyelination processes to initiate EAE [73]. Consistently, the $T^{\Delta NPGPx/\Delta NPGPx}$ mice showed increased numbers of spinal-infiltrated Th1 and Th17 cells (Fig. 3D–E), and had the earlier onset of EAE than that of control mice (Fig. 3A). Also, deficiency of other TCR negative regulator was also reported with earlier EAE onset [74]. These results support the notion that the fine-tune mechanisms of ZAP70 play imperative roles in maintaining the immune integrity, and could partially explain the immune disorders and autoimmune-liked phenotypes in whole-body NPGPx knockout mice [31].

In conclusion, we demonstrated herein that NPGPx modulates ZAP70 recruitment to TCR/CD3 complex through redox switching and prevents T cell hyperactivation upon TCR stimulation. This novel redox mechanism for modulation of ZAP70 activity casts new light on understanding the oxidative regulation of TCR signaling, providing a potential

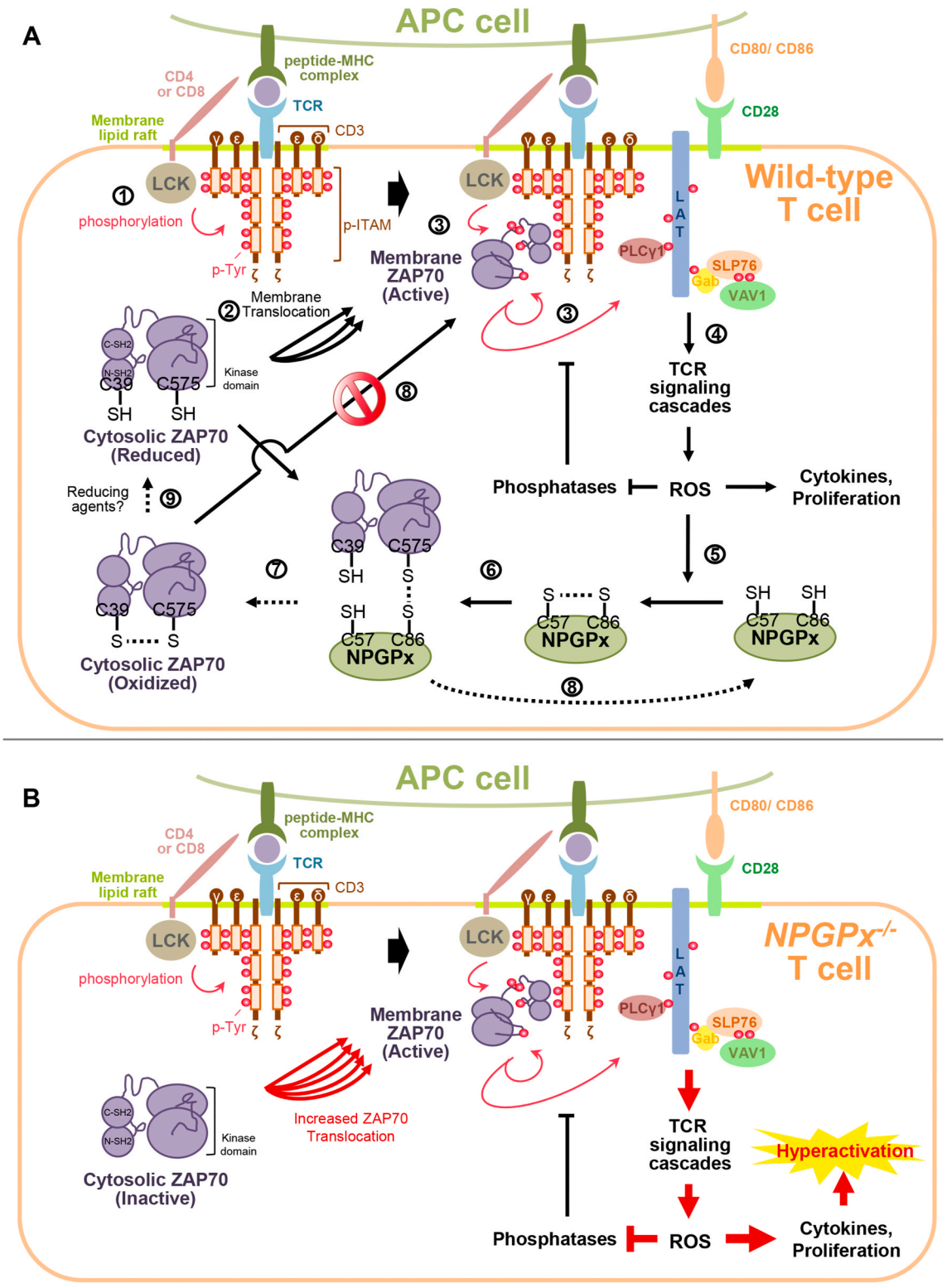

Fig. 8. Hypothetic model of NPGPx-mediated restriction of ZAP70 translocation upon TCR stimulation to eliminate T cell activation.
Proposed model of NPGPx-mediated ZAP70 modulation upon TCR stimulation: **(A)** In wild-type T cell, (1) peptide-MHC/TCR engagement promotes LCK activation to phosphorylate CD3-ITAMs, (2) which recruiting cytosolic ZAP70 translocation to enter lipid raft and bind p-ITAM. (3) The p-ITAM-binding ZAP70 is activated by LCK- and trans-autophosphorylation, (4) resulting in signal transfer to distinct substrates, provoking TCR signaling cascades and ROS production to suppress phosphatases, induce cytokine production, and activate cell proliferation. (5) In response to that, NPGPx senses TCR-induced ROS and confers to oxidized form. (6) Oxidized NPGPx attacks the Cys575 of remaining cytosolic ZAP70, (7) promoting the disulfide bond shuffling from NPGPx to ZAP70. (8) The oxidized ZAP70 is unable to be recruited to the TCR/CD3 complex and NPGPx can be recycled. (9) The oxidized ZAP70 might be relief by other reducing agents to reactivate its activity. **(B)** In NPGPx-deficient cell, the membrane translocation of ZAP70 is uncontrolled upon TCR stimulation, contributing to elevated TCR signaling and T cell hyperactivation.

therapeutic mechanism through blocking the NPGPx-ZAP70 regulatory axis in the treatment of T cell-related diseases, such as autoimmunity, inflammation, and cancer.

Data availability statement

All data that support the findings in this study are available from the corresponding author upon reasonable request. The mass spectrometry proteomics data have been deposited to the ProteomeXchange Consortium via the PRIDE partner repository [75] with the dataset identifier PXD017034 and PXD017046.

Ethics statement

Animal protocols were approved by the Institutional Animal Care and Use Committee (IACUC, protocol# 15-12-896) of Academia Sinica. The clinical study was approved by the institutional review board of the China Medical University Hospital (IRB no. CMUH103-REC2-127), and written informed consent was obtained from all subjects.

Author contributions

F-YS, S–CH, and W-HL designed the experiments. F-YS, S–CH, P-CW, and Y-LH conducted experiments and interpreted data. Y-LH provided plasmids. F-YS, L-WS, C-YC, and C-YY conducted animal experiments, animal breeding and housing. P-HH preformed and analyzed the mass spectrum analysis for disulfide bonding profiling. J-LH conducted the mass spectrum experiment in Supplementary Fig. 12F. J-PL, J-LL, EY-H-PL, and H-KS assisted in the experimental design and commented the manuscript. C-MH, J-YS, and W-HL coordinated experiments. F-YS, S–CH, and W-HL wrote and completed the manuscript.

Sources of funding

This research work was supported by funds from Academia Sinica, Taiwan (2371, 4012, AS-SUMMIT-109, and AS-KPQ-109-BioMed), and grants from Ministry of Science and Technology, Taiwan (MOST 104-0210-01-09-02, MOST 105-0210-01-13-01, MOST 106-0210-01-15-02, and MOST-108-3114-Y-001-002), higher education sprout project by the Ministry of Education, Taiwan, and funds from Philips Morris Foundation, USA.

Declaration of competing interest

The authors have declared that no conflict of interest exists.

Acknowledgments

We thank Dr. Yi-Hsuan Hsieh for her initial contribution to this work. We thank Dr. Der-Yen Li (Graduate Institute of Integrated Medicine, China Medical University, Taiwan), Dr. Che Alex Ma (Genomics Research Center, Academia Sinica, Taiwan), and Mrs. Jennifer Ming Lo (Genomics Research Center, Academia Sinica, Taiwan) in their kindly supports during the revision. We thank Dr. Fang Liao (Institute of Biomedical Sciences, Academia Sinica, Taiwan) and Dr. Kuo-I Lin (Genomics Research Center, Academia Sinica, Taiwan) for their critical comments of the manuscript. We thank the technical services provided by the "Transgenic Mouse Model Core Facility of the National Core Facility Program for Biotechnology, Ministry of Science and Technology, Taiwan" and the "Gene Knockout Mouse Core Laboratory of National Taiwan University Center of Genomic Medicine" for the transgenic mice construction, and the "GRC Mass Spectrometry Facility, Academia Sinica, Taiwan" for the mass spectrum service.

Appendix A. Supplementary data

Supplementary data to this article can be found online at https://doi.org/10.1016/j.freeradbiomed.2021.01.013.

References

[1] T. Finkel, N.J. Holbrook, Oxidants, oxidative stress and the biology of ageing, Nature 408 (2000) 239.
[2] K.M. Holmström, T. Finkel, Cellular mechanisms and physiological consequences of redox-dependent signalling, Nat. Rev. Mol. Cell Biol. 15 (2014) 411.
[3] C.R. Reczek, N.S. Chandel, ROS-dependent signal transduction, Curr. Opin. Cell Biol. 33 (2015) 8–13.
[4] Y.-M. Go, J.D. Chandler, D.P. Jones, The cysteine proteome, Free Radic. Biol. Med. 84 (2015) 227–245.
[5] M.M. Delmastro, J.D. Piganelli, Oxidative stress and redox modulation potential in type 1 diabetes, Clin. Dev. Immunol. (2011) 2011.
[6] M. Hultqvist, L.M. Olsson, K.A. Gelderman, R. Holmdahl, The protective role of ROS in autoimmune disease, Trends Immunol. 30 (2009) 201–208.
[7] O. Elena, M. Angela, D. Federica, C. Tania, G. Antonello, P. Marina, Relationship between redox status and cell fate in immunity and autoimmunity, Antioxidants Redox Signal. 21 (2014) 103–122.
[8] J. Kwon, K.E. Shatynski, H. Chen, S. Morand, X. de Deken, F. Miot, T.L. Leto, M. S. Williams, The nonphagocytic NADPH oxidase Duox1 mediates a positive feedback loop during T cell receptor signaling, Sci. Signal. 3 (2010) ra59-ra59.
[9] A. Sena Laura, S. Li, A. Jairaman, M. Prakriya, T. Ezponda, A. Hildeman David, C.-R. Wang, T. Schumacker Paul, D. Licht Jonathan, H. Perlman, et al., Mitochondria are required for antigen-specific T cell activation through reactive oxygen species signaling, Immunity 38 (2013) 225–236.
[10] S.H. Jackson, S. Devadas, J. Kwon, L.A. Pinto, M.S. Williams, T cells express a phagocyte-type NADPH oxidase that is activated after T cell receptor stimulation, Nat. Immunol. 5 (2004) 818.
[11] S. Devadas, L. Zaritskaya, S.G. Rhee, L. Oberley, M.S. Williams, Discrete generation of superoxide and hydrogen peroxide by T cell receptor stimulation: selective regulation of mitogen-activated protein kinase activation and Fas ligand expression, J. Exp. Med. 195 (2002) 59–70.
[12] J. Kwon, C.K. Qu, J.S. Maeng, R. Falahati, C. Lee, M.S. Williams, Receptor-stimulated oxidation of SHP-2 promotes T-cell adhesion through SLP-76–ADAP, EMBO J. 24 (2005) 2331–2341.
[13] S.-P. Lu, M.-H. Lin Feng, H.-L. Huang, Y.-C. Huang, W.-I. Tsou, M.-Z. Lai, Reactive oxygen species promote raft formation in T lymphocytes, Free Radic. Biol. Med. 42 (2007) 936–944.
[14] A.J. Case, J.L. McGill, L.T. Tygrett, T. Shirasawa, D.R. Spitz, T.J. Waldschmidt, K. L. Legge, F.E. Domann, Elevated mitochondrial superoxide disrupts normal T cell development, impairing adaptive immune responses to an influenza challenge, Free Radic. Biol. Med. 50 (2011) 448–458.
[15] T.W. Mak, M. Grusdat, G.S. Duncan, C. Dostert, Y. Nonnenmacher, M. Cox, C. Binsfeld, Z. Hao, A. Brüstle, M. Itsumi, et al., Glutathione primes T cell metabolism for inflammation, Immunity 46 (2017) 675–689.
[16] H.M. Tse, T.C. Thayer, C. Steele, C.M. Cuda, L. Morel, J.D. Piganelli, C.E. Mathews, NADPH oxidase deficiency regulates Th lineage commitment and modulates autoimmunity, J. Immunol. (2010), https://doi.org/10.4049/jimmunol.1001472.
[17] J. Muri, S. Heer, M. Matsushita, L. Pohlmeier, L. Tortola, T. Fuhrer, M. Conrad, N. Zamboni, J. Kisielow, M. Kopf, The thioredoxin-1 system is essential for fueling DNA synthesis during T-cell metabolic reprogramming and proliferation, Nat. Commun. 9 (2018) 1851.
[18] D.M. Previte, E.C. O'Connor, E.A. Novak, C.P. Martins, K.P. Mollen, J.D. Piganelli, Reactive oxygen species are required for driving efficient and sustained aerobic glycolysis during CD4+ T cell activation, PLOS ONE 12 (2017), e0175549.
[19] D.G. Franchina, C. Dostert, D. Brenner, Reactive oxygen species: involvement in T cell signaling and metabolism, Trends Immunol. 39 (2018) 489–502.
[20] B.B. Au-Yeung, N.H. Shah, L. Shen, A. Weiss, ZAP-70 in signaling, biology, and disease, Annu. Rev. Immunol. 36 (2018) 127–156.
[21] H. Wang, T.A. Kadlecek, B.B. Au-Yeung, H.E.S. Goodfellow, L.-Y. Hsu, T. S. Freedman, A. Weiss, ZAP-70: an essential kinase in T-cell signaling, Cold Spring Harbor Perspect. Biol. 2 (2010).
[22] E. Arpaia, M. Shahar, H. Dadi, A. Cohen, C.M. Rolfman, Defective T cell receptor signaling and CD8+ thymic selection in humans lacking Zap-70 kinase, Cell 76 (1994) 947–958.
[23] A. Chan, T. Kadlecek, M. Elder, A. Filipovich, W. Kuo, M. Iwashima, T. Parslow, A. Weiss, ZAP-70 deficiency in an autosomal recessive form of severe combined immunodeficiency, Science 264 (1994) 1599–1601.
[24] M. Elder, D. Lin, J. Clever, A. Chan, T. Hope, A. Weiss, T. Parslow, Human severe combined immunodeficiency due to a defect in ZAP-70, a T cell tyrosine kinase, Science 264 (1994) 1596–1599.
[25] I. Negishi, N. Motoyama, K-i Nakayama, K. Nakayama, S. Senju, S. Hatakeyama, Q. Zhang, A.C. Chan, D.Y. Loh, Essential role for ZAP-70 in both positive and negative selection of thymocytes, Nature 376 (1995) 435.
[26] T.A. Kadlecek, N.S.C. van Oers, L. Lefrancois, S. Olson, D. Finlay, D.H. Chu, K. Connolly, N. Killeen, A. Weiss, Differential requirements for ZAP-70 in TCR signaling and T cell development, J. Immunol. 161 (1998) 4688–4694.
[27] M.H. Hatada, X. Lu, E.R. Laird, J. Green, J.P. Morgenstern, M. Lou, C.S. Marr, T. B. Phillips, M.K. Ram, K. Theriault, et al., Molecular basis for interaction of the protein tyrosine kinase ZAP-70 with the T-cell receptor, Nature 377 (1995) 32–38.

[28] M.L. Dustin, D. Depoil, New insights into the T cell synapse from single molecule techniques, Nat. Rev. Immunol. 11 (2011) 672.
[29] E.C. Jury, F. Flores-Borja, P.S. Kabouridis, Lipid rafts in T cell signalling and disease, Semin. Cell Dev. Biol. 18 (2007) 608–615.
[30] I. Nakashima, K. Takeda, Y. Kawamoto, Y. Okuno, M. Kato, H. Suzuki, Redox control of catalytic activities of membrane-associated protein tyrosine kinases, Arch. Biochem. Biophys. 434 (2005) 3–10.
[31] P.-C. Wei, Y.-H. Hsieh, M.-I. Su, X. Jiang, P.-H. Hsu, W.-T. Lo, J.-Y. Weng, Y.-M. Jeng, J.-M. Wang, P-l Chen, et al., Loss of the oxidative stress sensor NPGPx compromises GRP78 chaperone activity and induces systemic disease, Mol. Cell 48 (2012) 747–759.
[32] A. Utomo, X. Jiang, S. Furuta, J. Yun, D.S. Levin, Y.-C.J. Wang, K.V. Desai, J. E. Green, P.-L. Chen, W.-H. Lee, Identification of a novel putative non-selenocysteine containing phospholipid hydroperoxide glutathione peroxidase (NPGPx) essential for alleviating oxidative stress generated from polyunsaturated fatty acids in breast cancer cells, J. Biol. Chem. 279 (2004) 43522–43529.
[33] W. Lei, Z. Lihui, N. Yingbo, S. Roberto, W. Chih-chen, Glutathione peroxidase 7 utilizes hydrogen peroxide generated by Ero1α to promote oxidative protein folding, Antioxidants Redox Signal. 20 (2014) 545–556.
[34] P.-J. Chen, J.-Y. Weng, P.-H. Hsu, J.-Y. Shew, Y.-S. Huang, W.-H. Lee, NPGPx modulates CPEB2-controlled HIF-1α RNA translation in response to oxidative stress, Nucleic Acids Res. 43 (2015) 9393–9404.
[35] P.P. Lee, D.R. Fitzpatrick, C. Beard, H.K. Jessup, S. Lehar, K.W. Makar, M. Pérez-Melgosa, M.T. Sweetser, M.S. Schlissel, S. Nguyen, et al., A critical role for Dnmt1 and DNA methylation in T cell development, function, and survival, Immunity 15 (2001) 763–774.
[36] R.C. Rickert, J. Roes, K. Rajewsky, B lymphocyte-specific, Cre-mediated mutagenesis in mice, Nucleic Acids Res. 25 (1997) 1317–1318.
[37] C.-Y. Chung, F. Liao, CXCR3 signaling in glial cells ameliorates experimental autoimmune encephalomyelitis by restraining the generation of a pro-Th17 cytokine milieu and reducing CNS-infiltrating Th17 cells, J. Neuroinflammation 13 (2016) 76.
[38] X. Zhang, R. Goncalves, D.M. Mosser, The isolation and characterization of murine macrophages, Curr. Protoc. Im. 14 (2008) 11, 11-14.11. 14.
[39] K. Inaba, W.J. Swiggard, R.M. Steinman, N. Romani, G. Schuler, C. Brinster, Isolation of dendritic cells, Curr. Protoc. Im. 3 (7) (2009) 1–3, 7. 19.
[40] J. Hasbold, A.B. Lyons, M.R. Kehry, P.D. Hodgkin, Cell division number regulates IgG1 and IgE switching of B cells following stimulation by CD40 ligand and IL-4, Eur. J. Immunol. 28 (1998) 1040–1051.
[41] B. Liu, Z. Li, Endoplasmic reticulum HSP90b1 (gp96, grp94) optimizes B-cell function via chaperoning integrin and TLR but not immunoglobulin, Blood 112 (2008) 1223–1230.
[42] V.K. Kuchroo, A.C. Anderson, H. Waldner, M. Munder, E. Bettelli, L.B. Nicholson, T cell response in experimental autoimmune encephalomyelitis (EAE): role of self and cross-reactive antigens in shaping, tuning, and regulating the autopathogenic T cell repertoire, Annu. Rev. Immunol. 20 (2002) 101–123.
[43] D.R. Fernandez, T. Telarico, E. Bonilla, Q. Li, S. Banerjee, F.A. Middleton, P. E. Phillips, M.K. Crow, S. Oess, W. Muller-Esterl, et al., Gene Expression Omnibus GSE13887, 2009, p. GDS4719. https://www.ncbi.nlm.nih.gov/geo/query/acc.cgi?acc=GSE13887.
[44] D.R. Fernandez, T. Telarico, E. Bonilla, Q. Li, S. Banerjee, F.A. Middleton, P. E. Phillips, M.K. Crow, S. Oess, W. Muller-Esterl, et al., Activation of mammalian target of rapamycin controls the loss of TCRζ in lupus T cells through HRES-1/Rab4-regulated lysosomal degradation, J. Immunol. 182 (2009) 2063–2073.
[45] L. Wang, L. Zhang, Y. Niu, R. Sitia, C-c Wang, Glutathione peroxidase 7 utilizes hydrogen peroxide generated by Ero1α to promote oxidative protein folding, Antioxidants Redox Signal. 20 (2014) 545–556.
[46] Y.C. Chang, Y.H. Yu, J.Y. Shew, W.J. Lee, J.J. Hwang, Y.H. Chen, Y.R. Chen, P. C. Wei, L.M. Chuang, W.H. Lee, Deficiency of NPGPx, an oxidative stress sensor, leads to obesity in mice and human, EMBO Mol. Med. 5 (2013) 1165–1179.
[47] C. Thurm, M.P. Poltorak, E. Reimer, M.M. Brinkmann, L. Leichert, B. Schraven, L. Simeoni, A highly conserved redox-active Mx((2))CWx((6))R motif regulates Zap70 stability and activity, Oncotarget 8 (2017) 30805–30816.
[48] P.W. Janes, S.C. Ley, A.I. Magee, Aggregation of lipid rafts accompanies signaling via the T cell antigen receptor, J. Cell Biol. 147 (1999) 447–461.
[49] K. Simons, D. Toomre, Lipid rafts and signal transduction, Nat. Rev. Mol. Cell Biol. 1 (2000) 31.
[50] R. Griffiths Helen, R. Dunston Christopher, J. Bennett Stuart, M. Grant Melissa, C. Phillips Darren, D. Kitas George, Free radicals and redox signalling in T-cells during chronic inflammation and ageing, Biochem. Soc. Trans. 39 (2011) 1273–1278.
[51] R.D. Michalek, K.J. Nelson, B.C. Holbrook, J.S. Yi, D. Stridiron, L.W. Daniel, J. S. Fetrow, S.B. King, L.B. Poole, J.M. Grayson, The requirement of reversible cysteine sulfenic acid formation for T cell activation and function, J. Immunol. 179 (2007) 6456–6467.
[52] M. Kamiński, M. Kießling, D. Süss, P.H. Krammer, K. Gülow, Novel role for mitochondria: protein kinase Cθ-dependent oxidative signaling organelles in activation-induced T-cell death, Mol. Cell Biol. 27 (2007) 3625–3639.
[53] N. Carpino, S. Turner, D. Mekala, Y. Takahashi, H. Zang, T.L. Geiger, P. Doherty, J. N. Ihle, Regulation of ZAP-70 activation and TCR signaling by two related proteins, Sts-1 and Sts-2, Immunity 20 (2004) 37–46.
[54] A. Mikhailik, B. Ford, J. Keller, Y. Chen, N. Nassar, N. Carpino, A phosphatase activity of Sts-1 contributes to the suppression of TCR signaling, Mol. Cell 27 (2007) 486–497.
[55] M. Yang, T. Chen, X. Li, Z. Yu, S. Tang, C. Wang, Y. Gu, Y. Liu, S. Xu, W. Li, et al., K33-linked polyubiquitination of Zap70 by Nrdp1 controls CD8+ T cell activation, Nat. Immunol. 16 (2015) 1253.
[56] R. Visperas Patrick, A. Winger Jonathan, M. Horton Timothy, H. Shah Neel, J. Aum Diane, A. Tao, T. Barros, Q. Yan, G. Wilson Christopher, R. Arkin Michelle, et al., Modification by covalent reaction or oxidation of cysteine residues in the tandem-SH2 domains of ZAP-70 and Syk can block phosphopeptide binding, Biochem. J. 465 (2015) 149–161.
[57] M.L. Oo, T. Senga, A.A. Thant, A.R.M.R. Amin, P. Huang, N.N. Mon, M. Hamaguchi, Cysteine residues in the C-terminal lobe of Src: their role in the suppression of the Src kinase, Oncogene 22 (2003) 1411–1417.
[58] T. Senga, H. Hasegawa, M. Tanaka, M.A. Rahman, S. Ito, M. Hamaguchi, The cysteine-cluster motif of c-Src: its role for the heavy metal-mediated activation of kinase, Canc. Sci. 99 (2008) 571–575.
[59] A. Veillette, S. Dumont, M. Fournel, Conserved cysteine residues are critical for the enzymatic function of the lymphocyte-specific tyrosine protein kinase p56lck, J. Biol. Chem. 268 (1993) 17547–17553.
[60] M.J. Wood, G. Storz, N. Tjandra, Structural basis for redox regulation of Yap1 transcription factor localization, Nature 430 (2004) 917–921.
[61] C.S. Sevier, H. Qu, N. Heldman, E. Gross, D. Fass, C.A. Kaiser, Modulation of cellular disulfide-bond formation and the ER redox environment by feedback regulation of Ero1, Cell 129 (2007) 333–344.
[62] T. Suzuki, A. Muramatsu, R. Saito, T. Iso, T. Shibata, K. Kuwata, S-i Kawaguchi, T. Iwawaki, S. Adachi, H. Suda, et al., Molecular mechanism of cellular oxidative stress sensing by Keap1, Cell Rep. 28 (2019) 746–758, e744.
[63] H.Y. Won, J.H. Sohn, H.J. Min, K. Lee, H.A. Woo, Y.-S. Ho, J.W. Park, S.G. Rhee, E. S. Hwang, Glutathione peroxidase 1 deficiency attenuates allergen-induced airway inflammation by suppressing Th2 and Th17 cell development, Antioxidants Redox Signal. 13 (2010) 575–587.
[64] M. Matsushita, S. Freigang, C. Schneider, M. Conrad, G.W. Bornkamm, M. Kopf, T cell lipid peroxidation induces ferroptosis and prevents immunity to infection, J. Exp. Med. 212 (2015) 555–568.
[65] A. Delaunay, D. Pflieger, M.-B. Barrault, J. Vinh, M.B. Toledano, A thiol peroxidase is an H2O2 receptor and redox-transducer in gene activation, Cell 111 (2002) 471–481.
[66] Y.-L. Hsieh, F.-Y. Su, L.-K. Tsai, C.-C. Huang, Y.-L. Ko, L.-W. Su, K.-Y. Chen, H.-M. Shih, C.-M. Hu, W.-H. Lee, NPGPx-mediated adaptation to oxidative stress protects motor neurons from degeneration in aging by directly modulating O-GlcNAcase, Cell Rep. 29 (2019) 2134–2143, e2137.
[67] J.-L. Hsu, J.-W. Chou, T.-F. Chen, J.-T. Hsu, F.-Y. Su, J.-L. Lan, P.-C. Wu, C.-M. Hu, E.Y.-H. Lee, W.-H. Lee, Glutathione peroxidase 8 negatively regulates caspase-4/11 to protect against colitis, EMBO Mol. Med. 12 (2020), e9386.
[68] J. Muri, H. Thut, G.W. Bornkamm, M. Kopf, B1 and marginal zone B cells but not follicular B2 cells require Gpx4 to prevent lipid peroxidation and ferroptosis, Cell Rep. 29 (2019) 2731–2744, e2734.
[69] H. Zhang, L. Wang, Y. Chu, Reactive oxygen species: the signal regulator of B cell, Free Radic. Biol. Med. 142 (2019) 16–22.
[70] J. Muri, H. Thut, S. Heer, C.C. Krueger, G.W. Bornkamm, M.F. Bachmann, M. Kopf, The thioredoxin-1 and glutathione/glutaredoxin-1 systems redundantly fuel murine B-cell development and responses, Eur. J. Immunol. 49 (2019) 709–723.
[71] N. Sakaguchi, T. Takahashi, H. Hata, T. Nomura, T. Tagami, S. Yamazaki, T. Sakihama, T. Matsutani, I. Negishi, S. Nakatsuru, et al., Altered thymic T-cell selection due to a mutation of the ZAP-70 gene causes autoimmune arthritis in mice, Nature 426 (2003) 454.
[72] A.Y. Chan, D. Punwani, T.A. Kadlecek, M.J. Cowan, J.L. Olson, E.F. Mathes, U. Sunderam, S. Man Fu, R. Srinivasan, J. Kuriyan, et al., A novel human autoimmune syndrome caused by combined hypomorphic and activating mutations in ZAP-70, J. Exp. Med. 213 (2016) 155–165.
[73] B.A. 't Hart, B. Gran, R. Weissert, EAE: imperfect but useful models of multiple sclerosis, Trends Mol. Med. 17 (2011) 119–125.
[74] J.-P. Li, C.-Y. Yang, H.-C. Chuang, J.-L. Lan, D.-Y. Chen, Y.-M. Chen, X. Wang, A. J. Chen, J.W. Belmont, T.-H. Tan, The phosphatase JKAP/DUSP22 inhibits T-cell receptor signalling and autoimmunity by inactivating Lck, Nat. Commun. 5 (2014) 3618.
[75] J.A. Vizcaíno, A. Csordas, N. del-Toro, J.A. Dianes, J. Griss, I. Lavidas, G. Mayer, Y. Perez-Riverol, F. Reisinger, T. Ternent, et al., 2016 update of the PRIDE database and its related tools, Nucleic Acids Res. 44 (2015) D447–D456.